Article

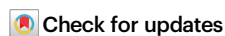# Suppression of multiple mouse models of refractory malignancies by reprogramming IL-18 ligand-receptor interaction

Zhen Fan[1,2,6], Ying Liu[3,6], Xueying Lin[2], Jifu Zhang[2], Jiehong Chen[1], Shiming Yi[2], Cheng Hu[4], Xincheng Liu[1], Cui Guo[1], Cuiying Xu[1], Xiaoyu Chen[1], Xuyan Tian[1], Xuanming Liang[1], Yang Liu[1], Linyi Hu[1], Shanyu Huang[1], Li Guo[1], Wenbo Zhu[1], Jun Hu[1], Guangmei Yan[1], Yuan Lin[1], Jing Cai[1,5] ✉ & Jiankai Liang[1,2] ✉

Achieving a cure is an urgent need for patients with advanced solid tumors. Here, we discover that oncolytic virus (OV) infection enhances IL-18 receptor expression but fails to increase IL-18 ligand expression. Therefore, we engineer armed oncolytic alphavirus M1 expressing wild-type IL-18 (wtIL-18) or a mutant variant (mutIL-18) that evades IL-18 binding protein (IL-18BP) while maintaining IL-18 receptor (IL-18R) binding. Intravenous administration of M1-mutIL-18 suppresses the growth of multiple advanced solid tumors in C57BL/6 and BALB/c mouse models and promotes long-term systemic immune memory. Mechanistically, armed M1-mutIL-18 enhances directed clonal expansion and differentiation of CD8$^+$ T cells and sustains IFN-γ production. Thus, armed M1-mutIL-18 promotes dendritic cell (DC) activation, priming and activation of CD8$^+$ T cells in lymphatic organs, and infiltration of IL-18R$^+$ CD8$^+$ T cells in the tumor microenvironment, establishing a positive feedback loop. We further show that a PD-L1 inhibitor enhances the anti-tumor efficacy of mutIL-18 OVs. These results highlight the importance of the IL-18 pathway in oncolytic virus therapy and implicate reprogramming ligand-receptor interaction as an effective strategy for immunotherapy.

Immunotherapy has significantly revolutionized the treatment landscape of malignant tumors in the last decade. Emerging immunotherapies such as immune checkpoint inhibitors and CAR-T cell therapy have demonstrated substantial clinical benefits for many patients, achieving complete responses in a subset without intolerable toxicities. However, a substantial proportion of patients still do not respond to these therapies. Data indicate that only 20−40% of patients respond to PD-1 antibody treatment[1,2], with only 5% achieving complete tumor remission[3] whereas CAR-T therapy primarily benefits patients with hematologic malignancies rather than solid tumors, leaving an unmet clinical need for non-responding solid tumor patients.

Oncolytic viruses (OV) represent a promising class of immunotherapy that selectively replicate within tumor cells, exposing the tumor antigens in situ by lysing tumor cells directly[4], and promoting the release of cytokines and damage- or pathogen-associated molecular patterns, thereby reprogramming an inflammatory tumor microenvironment (TME)[5]. OVs also serve as gene therapy vectors for delivering a wide range of transgenes, such as GM-CSF[6], HPGD[7], ICOS[8]

[1]Department of Pharmacology, Zhongshan School of Medicine, Sun Yat-sen University, Guangzhou 510080, China. [2]Department of Microbiology, Zhongshan School of Medicine, Sun Yat-sen University, Guangzhou 510080, China. [3]Department of Infectious Diseases, The Third Affiliated Hospital of Sun Yat-sen University, Guangzhou, Guangdong 510080, China. [4]Department of Urology, The Third Affiliated Hospital of Sun Yat-sen University, Guangzhou 510630, China. [5]Department of Molecular Biology and Biochemistry, Zhongshan School of Medicine, Sun Yat-sen University, Guangzhou 510080, China. [6]These authors contributed equally: Zhen Fan, Ying Liu. ✉e-mail: caij53@mail.sysu.edu.cn; liangjk5@mail.sysu.edu.cn

and leptin[9,10], which are specifically expressed in tumors to enhance the anti-tumor efficacy while minimizing systemic transgenes related adverse effects. Since the FDA approval of T-VEC for unresectable melanoma in 2015, oncolytic viruses have attracted lots of attention for their capacity to induce an inflammatory TME. In addition, the potential of OVs to enhance the antitumor effect of other immunotherapies has also reported and is currently undergoing clinical validation[11–15].

M1 virus, a naturally occurring positive single-stranded RNA virus of the alphavirus genus[16], has emerged as a novel oncolytic virus[17–19], with high tumor selectivity and robust replication in tumor tissues following intravenous administration[20,21]. M1 targeting of tumor cells is facilitated by the high expression of the virus receptor Mxra8 and the downregulation of the antiviral factor Zinc finger protein (ZAP) within tumor cells[22]. Subsequent reprogramming of the anti-tumor immunity in the TME also occurs after M1 infection, which can further promote the anti-tumor effect of PD-L1 antibody or dendritic cell (DC) vaccine[23,24]. Currently, Phase I clinical trials of oncolytic M1 for solid tumors are concurrently underway in China (NCT06368921) and Japan (NCT06046742) to investigate its safety profiles and antitumor potential in humans.

Here, we explore the potential of the M1 virus to treat advanced solid tumors resistant to immune checkpoint inhibitors. Our results show that M1 treatment significantly increases the infiltration of CD8$^+$ T cells and promotes the transformation of CD8$^+$ T cells from naïve T cells to effector T cells. We observe that following M1 virus infection, the expression of IL-18 receptor on the surface of effector T cells is upregulated, without significant changes in IL-18 ligands, and hypothesize that the absence of IL-18 ligands might limit the function of effector CD8$^+$ T cells and the efficacy of oncolytic virus M1. To exploit this discovery and exclude interference by IL-18BP, we use reverse genetics to arm M1 with a mutant IL-18, refractory to IL-18 binding protein. The armed M1-mutIL-18 virus promotes differentiation and clonal expansion of CD8$^+$ T cells, achieving complete regression in multiple advanced, treatment-refractory tumor models. These findings underscore the critical role of the IL-18 pathway in augmenting oncolytic virotherapy, and suggest that simultaneous targeting of the receptor and ligand achieves optimal efficacy. Thus, the reprogramming of ligand-receptor interactions using delivery vectors may enhance the effectiveness of cytokine-based therapeutic regimens in the clinic setting.

## Results

### Oncolytic virus upregulates IL-18 receptor expression in the TME

Our previous study demonstrated that the M1 virus effectively suppresses murine melanoma B16F10 in vivo and shapes the TME into an inflammatory state; however, its antitumor effect is not sustained[24]. In this study, we further evaluated the oncolytic efficacy of the M1 virus in the B16F10 mouse model, assessing its oncolytic effect in tumors with a larger initial burden. Similarly, M1 virus was observed to suppress tumor growth, however, complete tumor remission was not achieved (Fig. 1a). To identify the possible target to enhance the antitumor efficacy, we conducted further analysis of the TME immune status using single-cell RNA sequencing (scRNA-seq) of CD45$^+$ tumor-infiltrating leukocytes on day 7 post-M1 virus or PBS treatment in the B16F10 tumor model. Utilizing unsupervised clustering, we identified eleven distinct clusters of CD45$^+$ cells representing various cell populations based on known markers (Fig. 1b and Supplementary Fig. 1a). M1 virus induced notable changes in CD8$^+$ T cells, CD4$^+$ T cells, and B cells, with a marked increase in the proportion of CD8$^+$ T cells displaying enhanced expression of effector markers such as *Gzma*, *Gzmb*, *Gzmk*, and *Ifng* (Fig. 1b, c), consistent with previously reported CD8$^+$ T cell infiltration data[24]. Further analysis of CD8$^+$ T cells revealed five clusters (CD8$^+$ T naive, CD8$^+$ T

proliferating, CD8$^+$ T effector, CD8$^+$ T exhausted, CD8$^+$ T memory), showing a decrease in CD8$^+$ T naive cells and a significant amplification of CD8$^+$ T effector cells following M1 virus infection (Fig. 1d and Supplementary Fig. 1b).

Focusing on cytokine-related gene expressions in these CD8$^+$ T effector cells, we observed significant upregulation of chemokine receptors (*Ccr2*, *Ccr5*, *Cxcr3*, *Cxcr6*), effector IFN-γ, IL-18 receptors (*Il18r1* and *Il18rap*), TNF receptors (*Tnfrsf1a* and *Tnfrsf1b*), and IL-12 receptor *Il2rb1* compared to CD8$^+$ T naive cells (Fig. 1e). Consistent with these findings, M1 virus also induced the release of chemokines CXCL9, CCL12 and CXCL16 in the TME, which may result in increased infiltration of CD8$^+$ T cells (Fig. 1f). Transcriptome data also highlighted enhanced expression of IL-18 receptors (*Il18r1* and *Il18rap*), while the IL-18 ligand levels remained unchanged (Fig. 1g and Supplementary Data 1). Notably, *Il18r1* and *Il18rap* were predominantly expressed on activated CD8$^+$ T cells rather than naive CD8$^+$ T cells (Fig. 1h). We confirmed that M1 virus infection significantly reduced the proportion of naive CD8$^+$ T cells and promoted a substantial increase in activated CD8$^+$ T cells expressing enhanced IL-18Rα, despite no concurrent increase in IL-18 levels within the tumor (Fig. 1i, j and Supplementary Fig. 2). By analyzing the published RNA sequencing data, we found that oncolytic virus HSV-1 infection also enhanced the expression of IL-18 receptors on human tumors (Fig. 1k). Importantly, higher *Il18r1*, *Il18rap*, and *Il18* levels correlated with longer overall survival in melanoma patients (Fig. 1l). However, clinical outcomes with IL-18 treatment are limited[25–27], prompting the investigation of engineered 'decoy-resistant' IL-18 to enhance antitumor efficacy. This modified IL-18 is designed to evade binding by IL-18 binding protein (IL-18BP) and increase its affinity for IL-18 receptors[28]. As the analysis shows, IL-18 receptors were generally down-regulated on various solid tumors (Fig. 1m and Supplementary Fig. 3), suggesting that mere supplementation of IL-18 ligand may not achieve optimal antitumor effects.

Therefore, the upregulation of IL-18 receptors on CD8$^+$ T cells following M1 virus infection may present a promising target for IL-18 to maximize the therapeutic potential of increased CD8$^+$ T cell infiltration.

### Combination of OVs and IL-18 ligand synergistically enhances the antitumor efficacy

To test the above hypothesis, we utilized wild-type IL-18 (wtIL-18) or a mutant form (mutIL-18) in combination with M1 virus in tumor-bearing mouse models. MutIL-18, whose sequence is the same as the previously reported "decoy-resistant" IL-18, which evades IL-18BP while maintaining its binding capacity to the IL-18 receptor[28]. Either wtIL-18 or mutIL-18 combined with M1 virus demonstrated improved antitumor effects, with the mutIL-18 combination showing superior efficacy and prolonged survival (Fig. 2a, b). The combination of M1 virus with mutIL-18 also showed significant antitumor activity in CT26 colorectal tumor models (Fig. 2c). In line with the increased expression of IL-18 receptors following HSV-1 infection, HSV-1 also exhibited a synergistic effect with mutant IL-18, leading to sustained tumor remission in the CT26 tumor model (Fig. 2d).

Therefore, we engineered cytokine-loaded M1 viruses (M1-wtIL-18 and M1-mutIL-18) using alphavirus transducing method[29], with the loaded gene in between structural protein C and E3. These viruses effectively expressed functional wtIL-18 or mutIL-18 without compromising virus replication or antitumor efficacy in vitro (Fig. 2e–h and Supplementary Fig. 4a). In vivo validation demonstrated that M1-mutIL-18 virus showed enhanced tumor suppression in B16F10 models compared to M1 virus alone, whereas M1-wtIL-18 virus did not provide additional benefit (Fig. 2i, j). Mechanistically, the efficacy of M1-mutIL-18 virus relies on virus replication, as UV inactivation abolished its oncolytic effect (Fig. 2k, l). We speculate that the substantial release of IL-18 ligand in the TME due to virus replication may induce the expression of IL-18BP, thereby blocking immune
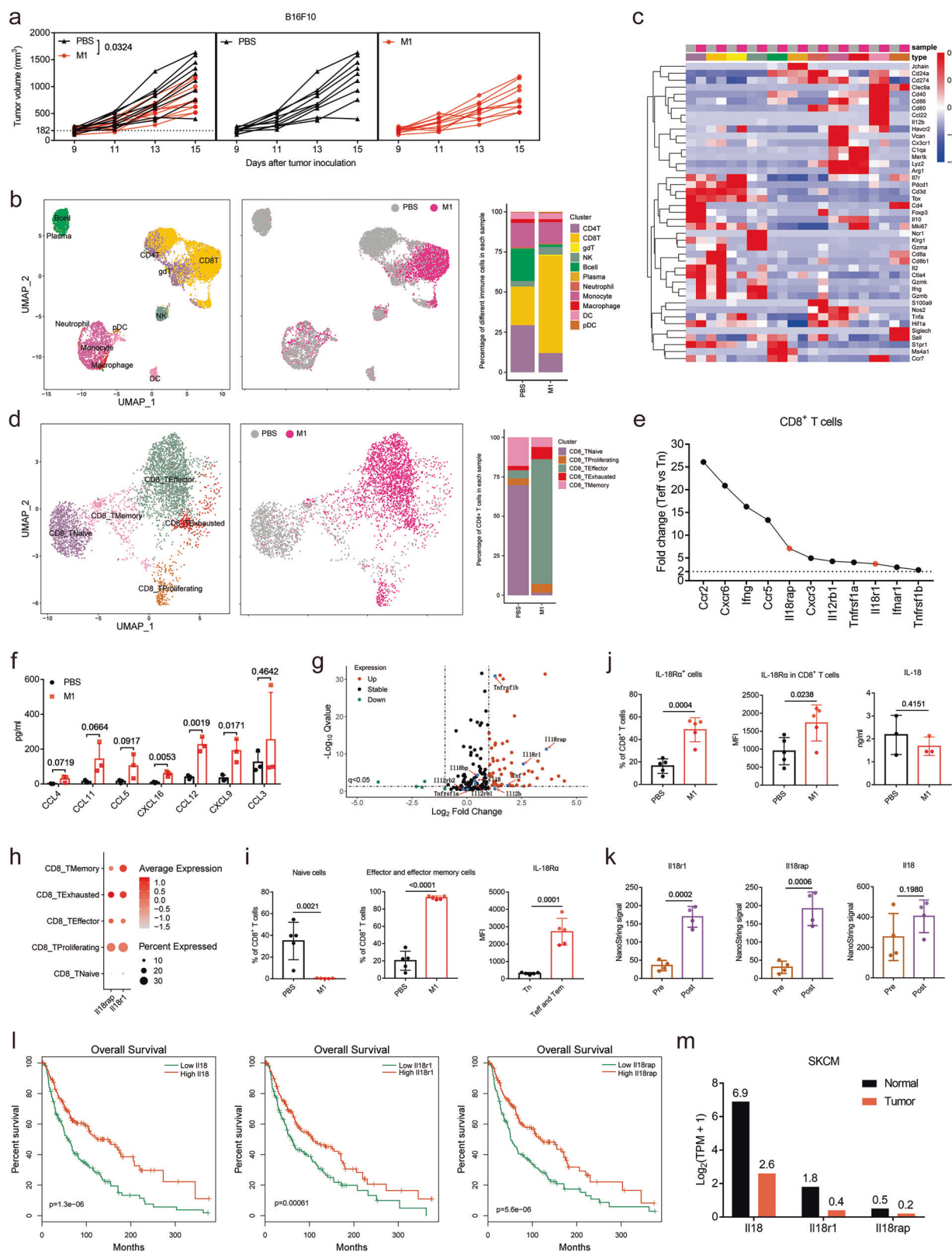
activation induced by wtIL-18 but not mutIL-18 (Supplementary Fig. 4b). Interestingly, incorporating mutIL-18 directly into the M1 virus genome yielded superior antitumor effects compared to combination therapy of M1 virus and mutIL-18 protein in both melanoma B16F10 model (Fig. 2m, n) and colorectal tumor CT26 model (Supplementary Fig. 5), showing that virus genome loading is a better way for leveraging IL-18 signaling.

## The potent antitumor effect of M1-mutIL-18 in multiple solid tumors

We further compared the antitumor efficacy of M1-mutIL-18 through intra-tumoral and intravenous administration. Surprisingly, intravenous injection of the M1-mutIL-18 virus exhibited comparable antitumor effects to intra-tumoral injection (Supplementary Fig. 6). Furthermore, intravenous administration of M1-mutIL-18 efficiently

**Fig. 1 | Oncolytic virus upregulates IL-18 receptor expression in the TME.**
**a** Female C57BL/6 J mice aged 4–6 weeks were implanted with B16F10 cells and treated with PBS or M1 (1.5 × 10$^7$ PFU) when tumor volumes were about 200 mm$^3$. PBS and M1 were administered via tail vein injection for 5 consecutive days. $n$ = 10 mice per group. **b–e, h** Single-cell RNA-seq data for about 10,000 CD45$^+$ sorted cells treated as in (**a**). **b** Distribution and frequency of different cluster in CD45$^+$ cells. **c** Expression of select genes in each cell cluster. **d** Distribution and frequency of different cluster in CD8$^+$ T cells. **e** Upregulated cytokine ligands and receptors in Teff compared to Tn. **f–j** Mice were treated as in (**a**). Mice were euthanized on the 3rd day after the last dose administration. The number of mice is the same as the individual data points in bar charts. **f** Changes in protein expression of chemokines after treatment with M1. **g** Changes in mRNA expression of cytokine receptors and ligands after treatment with M1. The fold change and $q$-value were calculated by DESeq. $n$ = 4 mice per group. **h** Expression of IL-18 receptor in different cluster of CD8$^+$ T cells. **i** Proportion of naïve cells, effector and effector memory cells in CD8$^+$ T cells and expression of IL-18Rα in naïve cells, effector and effector memory cells. **j** Changes in IL-18 receptors on CD8$^+$ T cells and IL-18 ligands. **k** Changes in IL-18 receptors and ligands in GBM patients after treatment with oHSV-1. GBM, Glioblastoma multiforme. $n$ = 4 patients per group. **l** Survival of SKCM patients with high or low expression of IL-18 receptor and ligand. SKCM, skin cutaneous melanoma. **m** Expression of IL-18 receptors and ligands transcripts in normal or tumor tissues from the TCGA database. In all figures, data with error bars represent mean ± SD. $P$-values were calculated using unpaired, two-tailed Student's $t$-test (**a–k**) or log rank test (**l**).

controlled not only small but also advanced-stage tumors (Fig. 3a, b and Supplementary Fig. 7a, b). Additionally, in a bilateral B16F10 tumor model, intravenous injection of M1-mutIL-18 elicited significant antitumor effects in both tumors (Supplementary Fig. 7c), highlighting its systemic therapeutic potential.

To further investigate the antitumor potential of M1-mutIL-18 across multiple solid tumors, we utilized three PD-1-resistant "cold" tumor models (breast tumor EMT6, malignant glioma GL261, and melanoma B16F10), and two PD-1-sensitive "hot" tumor models (colorectal tumor MC38 and CT26). Compared to the M1 virus, M1-mutIL-18 significantly suppressed tumor growth, extended overall survival, and cured some mice in all tested models (Fig. 3c–l). Importantly, M1-mutIL-18 did not exhibit overt toxicity, and the body weight of the mice remained stable during therapy (Supplementary Fig. 8). In CT26 tumor-bearing mice with complete response to M1-mutIL-18 treatment, we rechallenged with tumor cells on the same or opposite side of the original inoculation site about 100 days after cure. Tumor growth was inhibited in these mice, and similar results were observed even when rechallenged about 450 days after cure (Fig. 3m–r). Similar long-term tumor rejection upon M1-mutIL-18 treatment was also observed in B16F10 tumor-bearing mice model (Supplementary Fig. 9), strongly indicating the formation of antitumor immune memory post M1-mutIL-18 treatment.

These findings demonstrate that intravenous injection of M1-mutIL-18 virus effectively suppresses multiple solid tumors, irrespective of the immune status of the tumor microenvironment, and induces long-term antitumor immune memory to prevent tumor relapse.

## M1-mutIL-18 promotes rapid and intense activation of antitumor immunity

Since the receptors of IL-18 are mainly expressed on lymphocytes, we first investigated lymphocyte changes in the TME on day 4 or 7 following treatment with M1 or M1-mutIL-18. Data showed that M1-mutIL-18 treatment did not increase the infiltration of CD45$^+$ immune cells (Fig. 4a), the absolute number of CD8$^+$ T and CD4$^+$ T cells in the TME also remained stable on both day 4 and day 7 post M1-mutIL-18 treatment, but the infiltration of NK cell on day 4 was enhanced (Fig. 4b). In contrast, the proportion of CD8$^+$ T cells increased on both day 4 and day 7, while CD4$^+$ T cells, especially Treg cells, decreased in the TME (Fig. 4c, Supplementary Fig. 10a and Supplementary Fig. 10d). The ratios of CD8$^+$ T cells/Treg and conventional CD4$^+$ T cells /Treg, predictors of treatment efficacy, were also significantly increased (Fig. 4d). Functionally, the proportions of IFN-γ positive CD8$^+$ T cells, CD4$^+$ T cells, and NK cells were all significantly enhanced on day 4, and the proportions of IFN-γ positive CD4$^+$ T cells and NK cells remained elevated on day 7 (Fig. 4e and Supplementary Fig. 10b, e). The proportion of granzyme B-positive CD8$^+$ T cells, CD4$^+$ T cells, and NK cells was significantly increased on day 4 after M1-mutIL-18 treatment, and the MFI of granzyme B in these cells was also significantly elevated on day 4 (Fig. 4f and Supplementary Fig. 10b, e, f). While the enhancement of granzyme B in NK cells persisted until day 7, it declined in CD8$^+$

T cells and CD4$^+$ T cells. In contrast, although M1 virus significantly induced CD8$^+$ and CD4$^+$ T cell infiltration in the TME, the proportions of IFN-γ positive lymphocytes or the expression of granzyme B were markedly lower compared to the M1-mutIL-18 treatment, particularly decreasing by day 7 in CD8$^+$ cells (Fig. 4e, f and Supplementary Fig. 10e, f). TNF was primarily induced by M1 virus rather than M1-mutIL-18 (Supplementary Fig. 10b, g). Furthermore, the percentage of IFN-γ$^+$ TNF$^+$ CD8$^+$ T cells, which represents CD8$^+$ T cell polyfunctionality, was also significantly elevated on day 4, and returned to baseline levels by day 7 following M1-mutIL-18 or M1 treatment (Fig. 4g and Supplementary Fig. 10c). In contrast, the percentage of IFN-γ$^+$ TNF$^+$ CD4$^+$ T cell was substantially increased on both day 4 and day 7 (Supplementary Fig. 10c, h). Changes observed in splenic lymphocytes on day 7 after M1-mutIL-18 treatment approximately mirrored those in the TME (Supplementary Fig. 11). Furthermore, the memory marker CD44 on CD8$^+$ and CD4$^+$ T cells was significantly upregulated following M1-mutIL-18 treatment, and the proportion of tumor-specific CD39$^+$ CD44$^+$ CD8$^+$ T cells was also increased (Fig. 4h, i and Supplementary Fig. 10i–k). Consistently, lymphocytes isolated from lymph nodes and spleens of M1-mutIL-18-treated mice also demonstrated enhanced in vitro antitumor efficacy (Fig. 4j). These findings demonstrate a significant increase in anti-tumor immune cells following M1-mutIL-18 treatment.

## M1-mutIL-18 promotes the differentiation of T cells and directed clonal expansion of CD8$^+$ T cells

To further profile the immune status after M1-mutIL-18 infection, scRNA-seq and scTCR-seq of CD45$^+$ tumor-infiltrating leukocytes on day 7 were detected in the B16F10 model, combined with previous M1 and PBS data, 11 distinct cell clusters were identified (Supplementary Fig. 12a). As shown, compared to the PBS group, NK and CD8$^+$ T cell proportion were enhanced after M1-mutIL-18 treatment, while CD4$^+$ T cell proportion was decreased (Fig. 5a, b). Consistent with previous study, IL-18 receptors were mainly expressed on these lymphocytes, and the expression of *Ifng* was positively related to IL-18 receptor expressions (Supplementary Fig. 13). We also noticed that monocyte and macrophage numbers in the TME were significantly reduced (Fig. 5a, b, Supplementary Figs. 12b and 14). Given the immunosuppressive role of tumor-associated myeloid cells[30], this reduction likely contributes to the enhanced anti-tumor efficacy of M1-mutIL-18.

Further lymphocyte subdivision revealed that CD8$^+$ T cells in the M1-mutIL-18 group consisted of naïve, proliferating, effector, exhausted, and memory subsets, contrasting with the predominance of effector CD8$^+$ T cells in the M1 virus group (Fig. 5a, b and Supplementary Fig. 12b). Functional gene analysis showed lymphocyte activation following M1-mutIL-18 treatment, with the expression of functional molecules, such as *Ifng*, *Tnf* and *Gzmb*, increased in both effector and exhausted CD8$^+$ T cells (Fig. 5c and Supplementary Fig. 15). Interestingly, M1-mutIL-18 treatment increased the expression of *Gzmk* in both NK cells and CD8$^+$ T cells (Fig. 5a, b and Supplementary Fig. 15). Compared
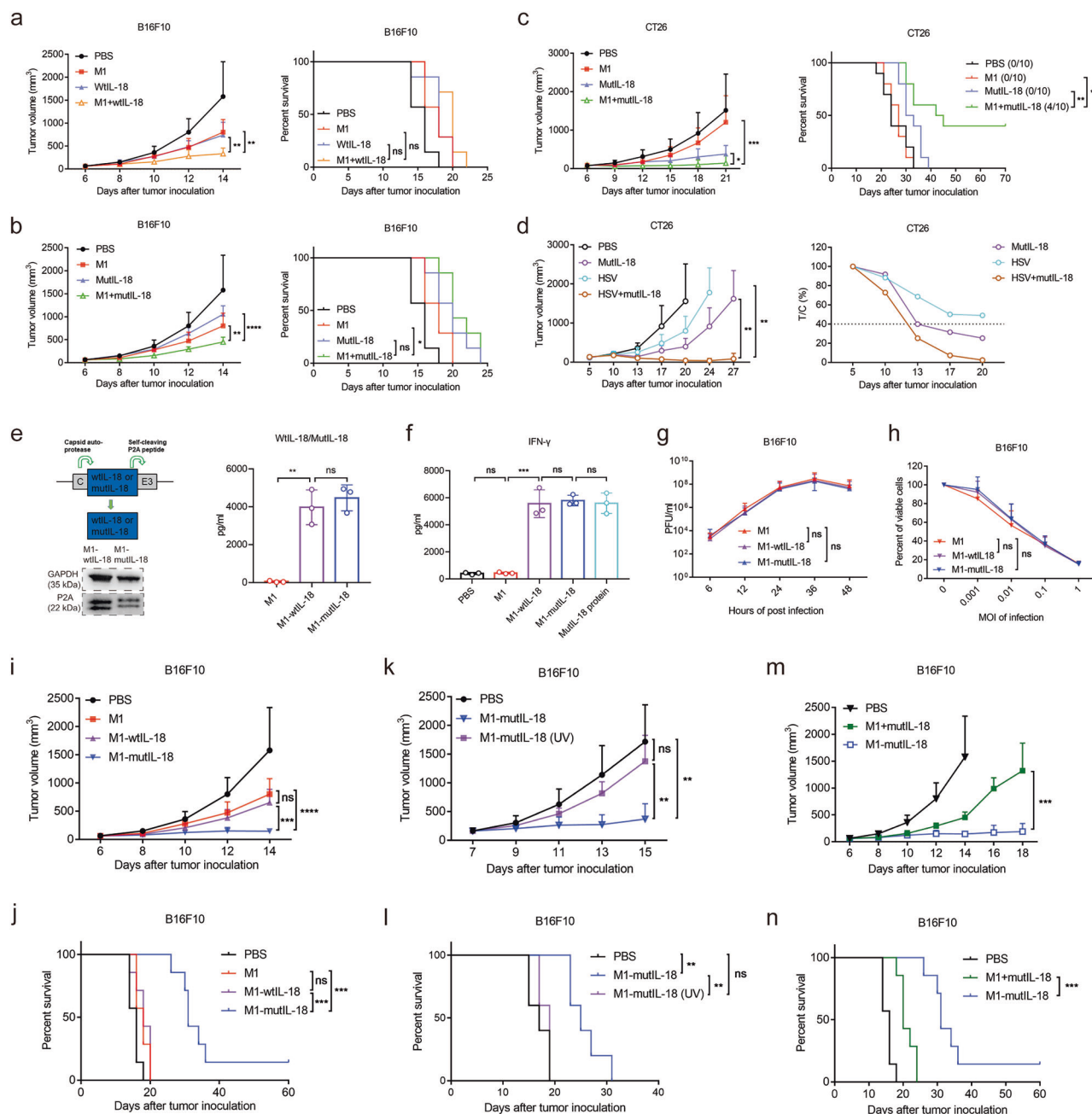
**Fig. 2 | Combination of OVs and IL-18 ligand synergistically enhances the antitumor efficacy. a−c** Female C57BL/6 J or BALB/c mice aged 4−6 weeks were implanted with B16F10 or CT26 cells and treated with PBS or M1 (1.5 × 10⁷ PFU) via tail vein injection for 5 consecutive days. On the day of the first administration of M1, wtIL-18 protein (0.32 mg/kg) and mutIL-18 (0.32 mg/kg) were intraperitoneally injected twice weekly for a total of 5 times. **a, b** n = 7 mice per group; **c**, n = 10 mice per group. **d** Female BALB/c mice aged 4−6 weeks were implanted with CT26 cells and treated with HSV-1 (2 × 10⁶ PFU) via a single intra-tumor injection. On the day of the administration of HSV-1, mutIL-18 (0.32 mg/kg) were intraperitoneally injected twice weekly for a total of 5 times. PBS, n = 3; Other groups, n = 4. **e** Construction of M1-wtIL-18 and M1-mutIL-18 and expression of wtIL-18 and mutIL-18 by B16F10 cells after infection with 0.001 MOI M1-wtIL-18 or M1-mutIL-18 for 48 h. **f** Activity of wtIL-18 (4 ng/mL, total 1 ml) and mutIL-18 (4 ng/mL, total 1 ml) expressed by M1-wtIL-18

and M1-mutIL-18 after infecting B16F10 cells. The mutIL-18 protein (4 ng/mL, total 1 ml) expressed by plasmid transformed into prokaryotes was used as a positive control. **g** Replication kinetics after infection of B16F10 cells with 0.01 MOI M1-wtIL-18 or M1-mutIL-18. **e−g** n = 3 biological replicates per group. **h** Cell viability after infection of B16F10 cells with different MOI M1-wtIL-18 or M1-mutIL-18 for 24 h. n = 4 biological replicates per group. **i, j** Efficacy of M1-wtIL-18 and M1-mutIL-18 treated as in (**a**). n = 7 mice per group. **k, l** Efficacy of UV-inactivated M1-mutIL-18 treated as in (**a**). n = 5 mice per group. UV, ultraviolet. **m, n** Efficacy of mutIL-18 protein in combination with M1 and M1-mutIL-18 treated as in (**a**). n = 7 mice per group. In all figures, data with error bars represent mean ± SD. ns, not significant. *P < 0.05, **P < 0.01, ***P < 0.001, ****P < 0.0001. P-values were calculated using unpaired, two-tailed Student's t-test (**a−f, i, k, m**), two-way ANOVA (**g, h**) or log rank test (**a−c, j, l, n**).

to the PBS group, the expression of *Gzmk* in CD8⁺ T cells was elevated across all subsets of CD8⁺ T cells following treatment with either M1-mutIL-18 or M1, implicating the enhanced cytotoxic potential of CD8⁺ T cells (Supplementary Figs. 15 and 16a−c). In addition, some studies have demonstrated that GZMK⁺ CD8⁺ T cells promote the release of pro-

inflammatory cytokines, such as IL-1β, IL-6, and IL-8, which may drive inflammation and contribute to the recruitment of neutrophils[31–33]. This is supported by our scRNA-seq data, which showed an increase in neutrophils following M1-mutIL-18 treatment (Fig. 5a, b and Supplementary Fig. 14).
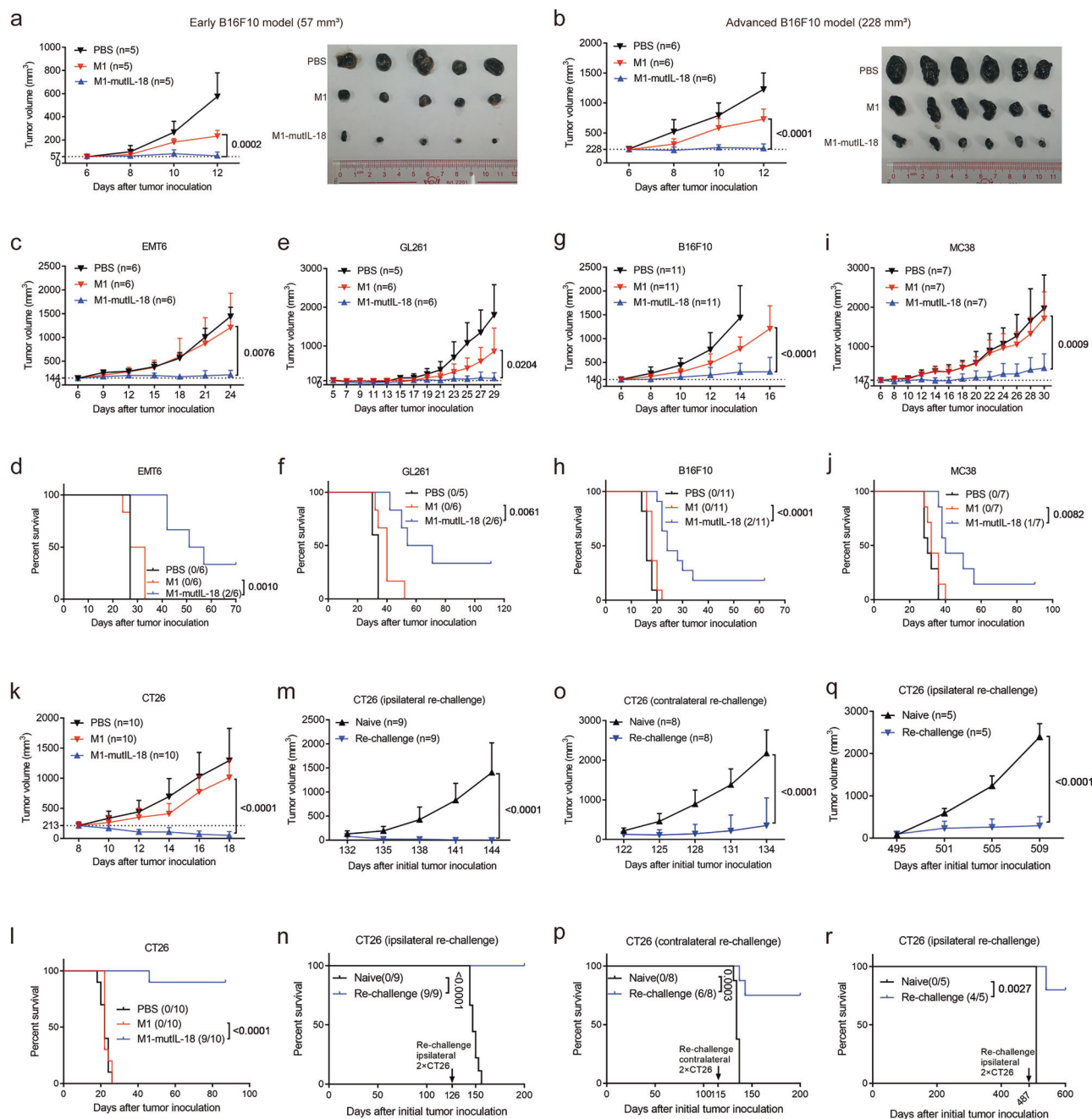
**Fig. 3 | The potent antitumor effect of M1-mutIL-18 in multiple solid tumors.** **a**−**l** Female C57BL/6 J or BALB/c mice aged 4−6 weeks were implanted with B16F10 cells (**a**, **b**) EMT6 cells (**c**, **d**) GL261 cells (**e**, **f**), B16F10 cells (**g**, **h**) MC38 cells (**i**, **j**) or CT26 cells (**k**, **l**) and treated with M1 ($1.5 \times 10^7$ PFU) or M1-mutIL-18 ($1.5 \times 10^7$ PFU) when the tumors reached the appropriate volume as shown in the figure. M1 or M1-mutIL-18 were administered via tail vein injection for 5 consecutive days. **m**−**r**, Mice re-challenged with twice the initial dose of CT26 tumor cells after successful M1-mutIL-18 treatment. **m**, **n** Mice were re-challenged on the ipsilateral of the cured site 126 days after initial tumor inoculation. **o**, **p** Mice were re-challenged on the contralateral of the cured site 115 days after initial tumor inoculation. **q**, **r** Mice were re-challenged on the ipsilateral of the cured site 487 days after initial tumor inoculation. **a**−**r** the number of mice is shown in the figure. In all figures, data with error bars represent mean ± SD. *P*-values were calculated using unpaired, two-tailed Student's *t*-test (**a**−**q**) or log rank test (**d**−**r**).

Pseudo-time analysis revealed that CD8+ T cells in the M1 virus group remained stagnated in the effector state, whereas those in the M1-mutIL-18 group successfully differentiated into exhausted, proliferative, and memory states, with exhausted CD8+ T cells being the dominant subset (Fig. 5d). we also observed that *Tox*, a critical transcription factor in T cell exhaustion[34], was obviously elevated across all CD8+ T cell subsets except naïve cells post M1-mutIL-18 treatment. However, further analysis revealed that despite the increased expression of inhibitory receptors and decreased expression of co-stimulatory immune receptors, these exhausted CD8+ T cells still exhibited high levels of *Ifng*, *Gzmb*, and *Tnf* (Fig. 5c and Supplementary Fig. 15). These results suggest the existence of a dual-phenotype CD8+ T cell subset, characterized by both exhaustion and cytotoxic effector signatures, a phenomenon previously reported in other studies[35-38].

TCR analysis revealed that naïve and memory CD8+ T cells experienced limited clonal expansion, where proliferating, effector and exhausted CD8+ T cells displayed greater clonal expansion (Fig. 6a). Enhanced clonal expansion of CD8+ T cells was observed after
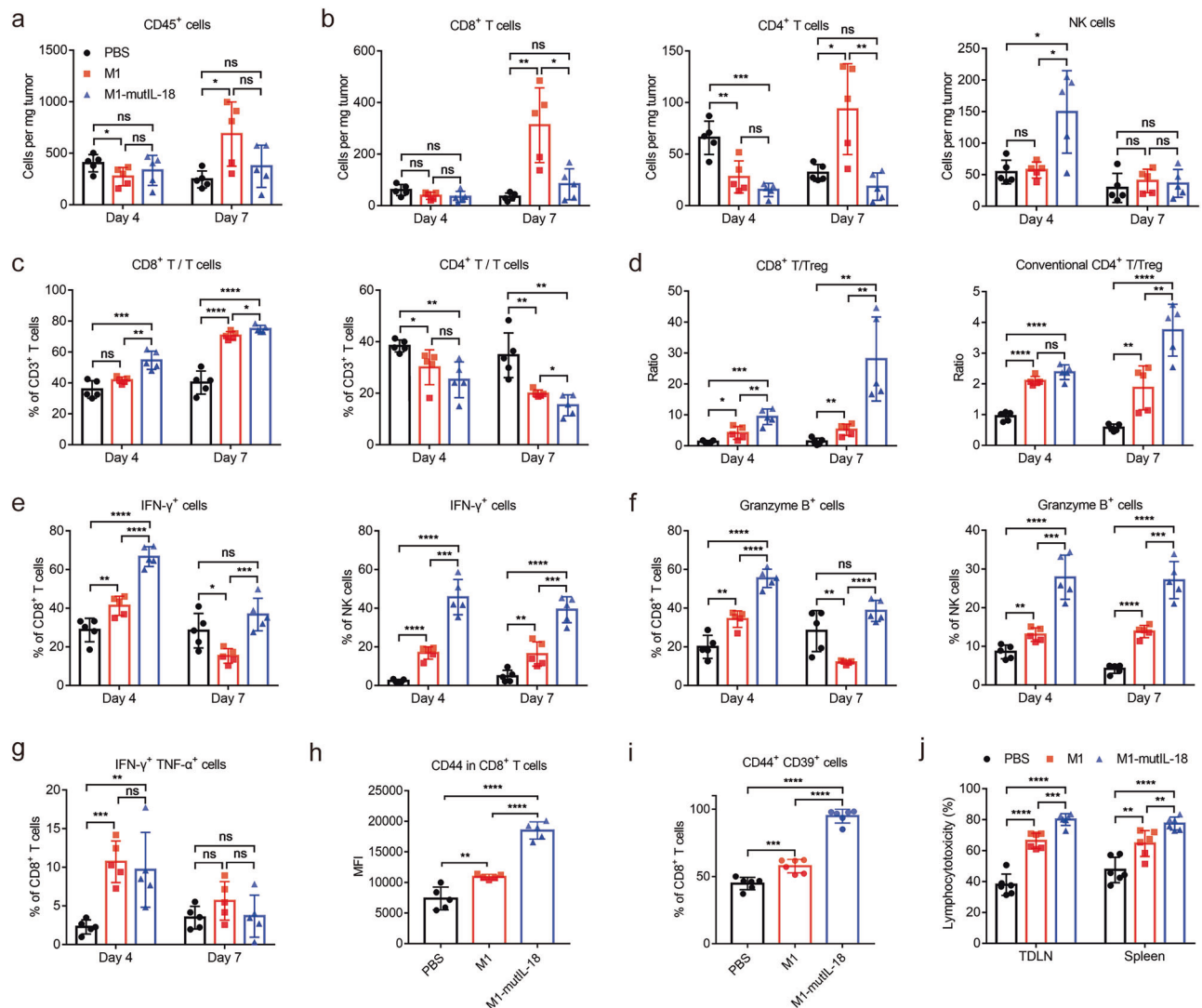
**Fig. 4 | M1-mutIL-18 promotes rapid and intense activation of anti-tumor immunity. a–i** Female C57BL/6 J mice aged 4–6 weeks were implanted with B16F10 cells and treated with M1 ($1.5 \times 10^7$ PFU) or M1-mutIL-18 ($1.5 \times 10^7$ PFU) via tail vein injection for 5 consecutive days. Mice were euthanized on day 4 and day 7 after the first dose administration. The number and function of immune cells in TME were analyzed by flow cytometry. **a** Absolute cell numbers of tumor-infiltrating CD45^{+} cells. **b** Absolute cell numbers of tumor-infiltrating CD8^{+} T cells, CD4^{+} T cells and NK cells. **c** Proportion of CD8^{+} T cells and CD4^{+} T cells in T cells. **d** Ratios of CD8^{+} T cells vs. Treg and conventional CD4^{+} T cells vs. Treg. **e** Proportion of IFN-γ^{+} cells in CD8^{+} T cells and NK cells. **f** Proportion of granzyme B^{+} cells in CD8^{+} T cells and NK cells.
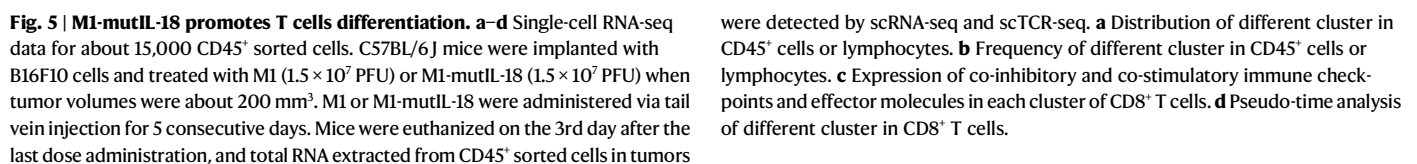
**g** Proportion of IFN-γ^{+} TNF^{+} cells in CD8^{+} T cells. **h** MFI of CD44 in CD8^{+} T cells. **i** Proportion of CD44^{+} CD39^{+} cells in CD8^{+} T cells. **j** Mice were treated as in (**a**). Lymphocytes isolated from tumor draining lymph nodes (tdLN) and spleen were cocultured with B16F10 cells in an E:T = 100:1 ratio for 72 h to evaluate lymphocy-totoxicity. **a–g** The figure legends are same as in Fig. 4a. **a–j** The number of mice is the same as the individual data points in bar charts. In all figures, data with error bars represent mean ± SD. ns, not significant. *$P < 0.05$, **$P < 0.01$, ***$P < 0.001$, ****$P < 0.0001$. P-values were calculated using unpaired, two-tailed Student's t-test (**a–j**).

M1 or M1-mutIL-18 treatment, however, M1 treatment induced higher TCR diversity in these clonally expanded CD8^{+} T cells (Fig. 6b). Notably, three clones exhibited significant expansion after M1-mutIL-18 treatment, comprising about 30% of the total CD8^{+} T cell population (Fig. 6b-d and Supplementary table 1). The aforementioned dual-phenotype CD8^{+} T cells were predominantly composed of these most expanded CD8^{+} T cells, which also simultaneously displayed exhausted and cytotoxic phenotype (Figs. 5c, 6e-g and Supplementary Data 2), suggesting that dual-phenotype CD8^{+} T cells may be highly differ-entiated terminal effector CD8^{+} T cells. Importantly, memory CD8^{+} T cells were successfully induced in all three major clones (Fig. 6e, f), ensuring sustained antitumor immunity after M1-mutIL-18 treatment.

Collectively, these data indicate that M1-mutIL-18 promotes the activation and differentiation of CD8^{+} T cells within the tumor microenvironment.

## CD8^{+} T cells, NK cells and IFN-γ mediate the antitumor effect of M1-mutIL-18

To ascertain the contribution of lymphocytes, we initially depleted CD8^{+} and CD4^{+} T cells in immunocompetent mice. In B16F10 model, we found that CD8^{+} T cell deletion partially reversed the antitumor effects of M1-mutIL-18, whereas CD4^{+} T cell deletion did not impact outcomes (Fig. 7a and Supplementary Fig. 17). Moreover, the results in rag1^{-/-} mice demonstrated that both M1 and M1-mutIL-18 prolonged survival, with M1-mutIL-18 exhibiting superior efficacy (Fig. 7b). However, upon NK cell depletion, the efficacy of M1 remained unchanged, whereas the efficacy of M1-mutIL-18 was significantly reduced, showing no difference compared to M1 alone (Fig. 7c). These data suggest that the benefit conferred by mutIL-18 requires NK cells, and the therapeutic benefit of the M1 virus itself may result from other mechanism, for example the direct oncolytic effect
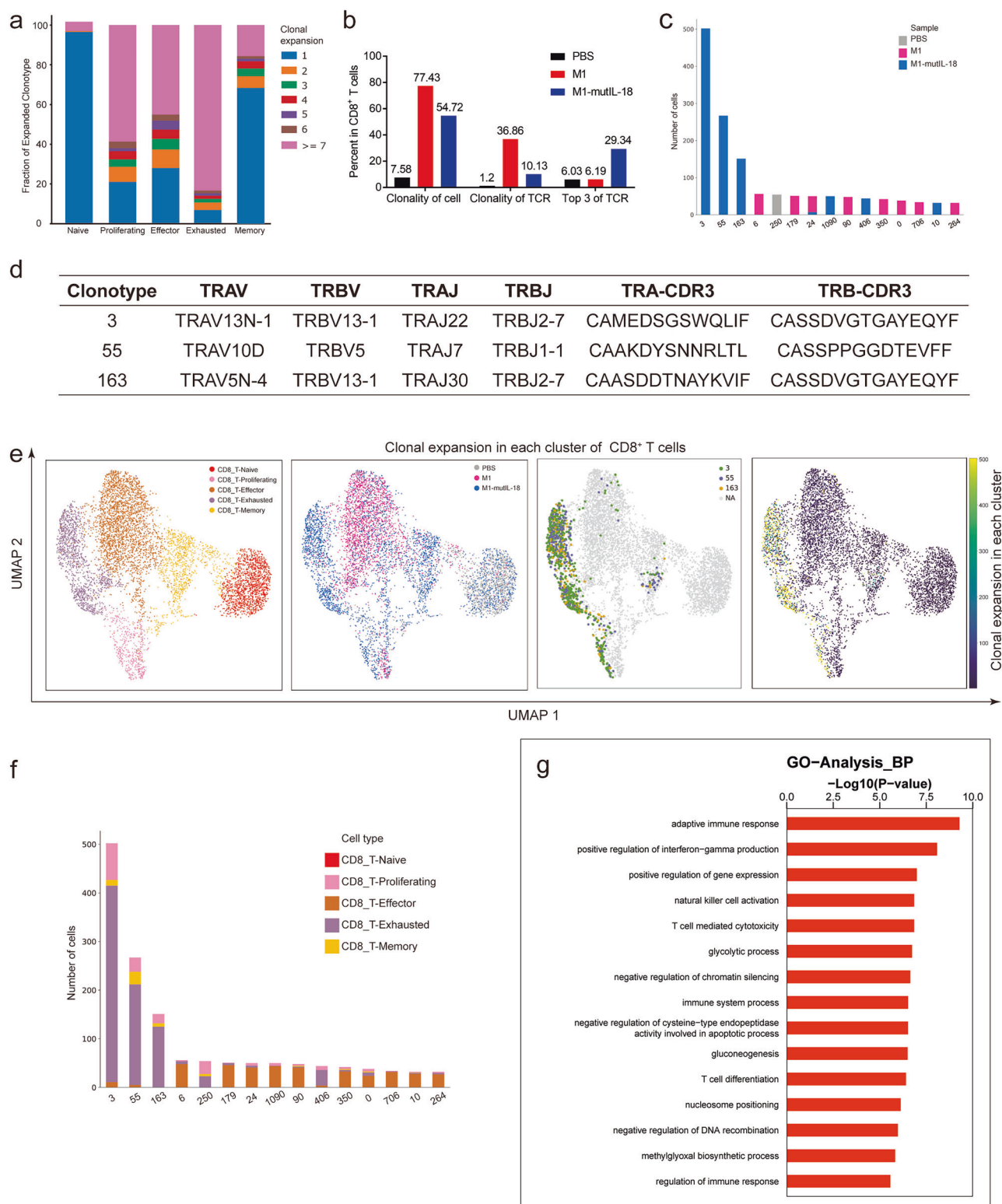
**Fig. 5 | M1-mutIL-18 promotes T cells differentiation. a–d** Single-cell RNA-seq data for about 15,000 CD45^{+} sorted cells. C57BL/6 J mice were implanted with B16F10 cells and treated with M1 (1.5 × 10^{7} PFU) or M1-mutIL-18 (1.5 × 10^{7} PFU) when tumor volumes were about 200 mm³. M1 or M1-mutIL-18 were administered via tail vein injection for 5 consecutive days. Mice were euthanized on the 3rd day after the last dose administration, and total RNA extracted from CD45^{+} sorted cells in tumors were detected by scRNA-seq and scTCR-seq. **a** Distribution of different cluster in CD45^{+} cells or lymphocytes. **b** Frequency of different cluster in CD45^{+} cells or lymphocytes. **c** Expression of co-inhibitory and co-stimulatory immune check-points and effector molecules in each cluster of CD8^{+} T cells. **d** Pseudo-time analysis of different cluster in CD8^{+} T cells.

**Fig. 6 | M1-mutIL-18 promotes directed clonal expansion of CD8⁺ T cells.**
**a** Clonal expansion of different cluster in CD8⁺ T cells. **b** Changes in TCR in CD8⁺ T cells in each group. **c** Clonal number of the top 15 TCRs in all groups. **d** Sequences of the most expanded TCRs across treatment conditions. **e** Distribution of clonally expanded CD8⁺ T cells. **f** Changes of differentiation in the top 15 TCRs in all groups. **g** Differential gene enrichment analysis of CD8⁺ T cells with top3 TCRs compared to CD8⁺ T cells without top3 TCRs in the M1-mutIL-18 group. *P*-values were calculated using Fisher's exact test and adjustments were made for multiple comparisons (**g**).

benefiting from compromised antiviral immunity in rag1⁻/⁻ mice[39–41]. In MC38 model, we found that the antitumor effect was completely canceled upon CD8⁺ T cell deletion, however, CD4⁺ T cell or NK cells deletion did not impact outcomes (Supplementary Fig. 18).

Furthermore, the antitumor effects of M1-mutIL-18 were completely abrogated upon IFN-γ neutralization in B16F10 model (Fig. 7d). These findings demonstrate that the infiltration and activation of NK cells and CD8⁺ T cells after M1-mutIL-18 infection induce potent and
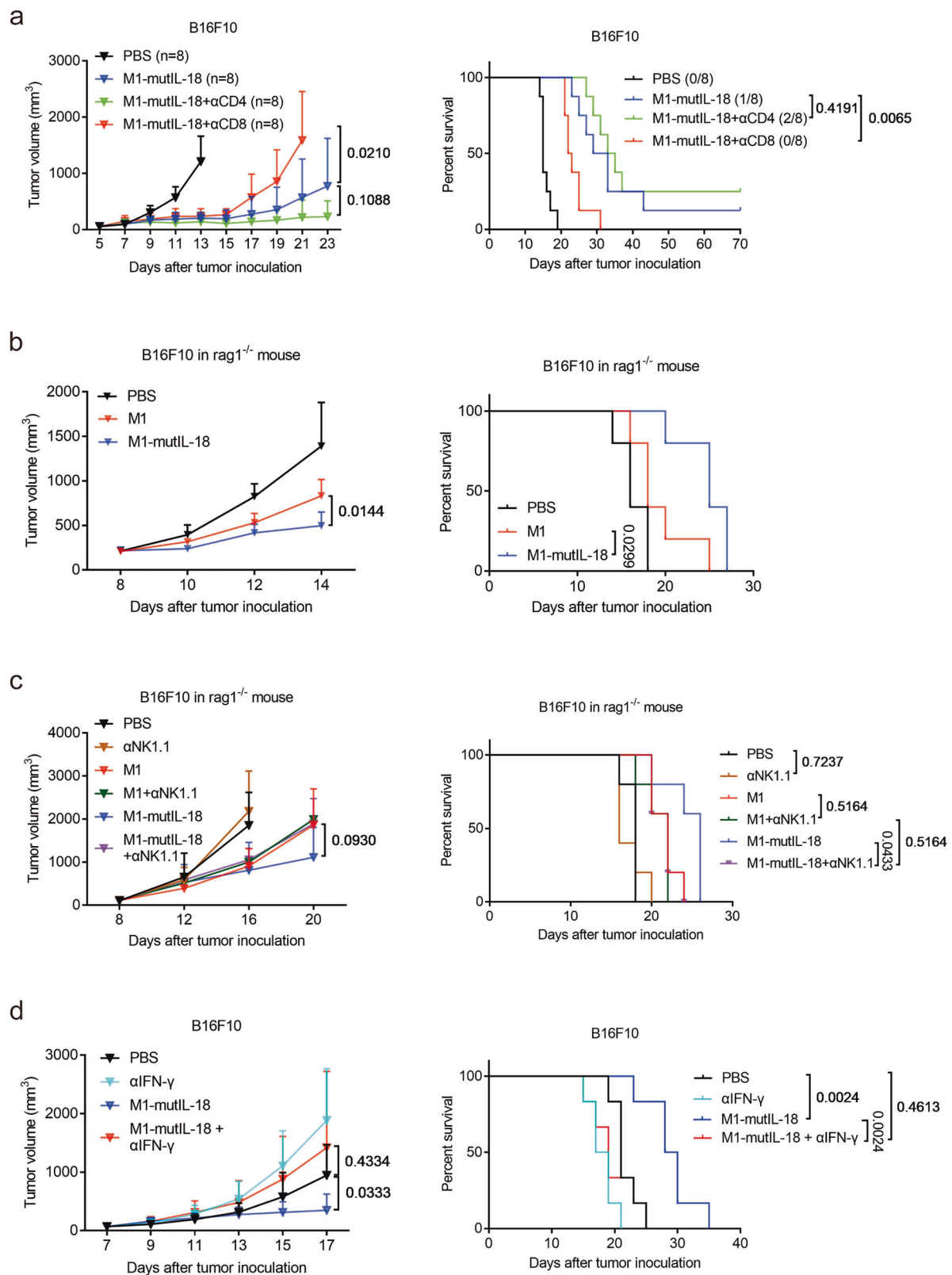
**Fig. 7 | CD8^{+} T cells, NK cells and IFN-γ mediate the antitumor effect of M1-mutIL-18. a–d** Female C57BL/6J mice (**a**, **d**), female rag1^{-/-} mice (**b**) and male rag1^{-/-} mice (**c**) aged 4–6 weeks were implanted with B16F10 cells and treated with M1 (a, $4 \times 10^6$ PFU; **b–d**, $1.5 \times 10^7$ PFU) or M1-mutIL-18 (a, $4 \times 10^6$ PFU; **b–d**, $1.5 \times 10^7$ PFU) via tail vein injection for 5 consecutive days. For depletion study, CD8 antibody, CD4 antibody, NK1.1 antibody and IFN-γ antibody were intraperitoneally injected every

3 days for a total of 5 times. Antibodies were administered 2 days before oncolytic virus therapy. **a** $n = 8$ mice per group; **b**, **c** $n = 5$ mice per group; (**d**) $n = 6$ mice per group. In all figures, data with error bars represent mean ± SD. *P*-values were calculated using unpaired, two-tailed Student's *t*-test (**a–d**, tumor growth curves) and log rank test (**a–d**, Kaplan–Meier survival curves).

sustained release of IFN-γ, which exerts dominated anti-tumor effects.

## M1-mutIL-18 enhances IL-18 receptor on CD8+ T cells via DC and creates a positive feedback loop

IFN-γ exerts its antitumor effects by binding to its receptors, IFN-γR1 and IFN-γR2. Interestingly, we observed distinct expression patterns of IFN-γR2 among different immune cell subsets following M1-mutIL-18 treatment. Specifically, IFN-γR2 expression was found to be minimal on CD8+ T cells, decreased on CD4+ T cells and NK cells, and significantly elevated on DCs and macrophages, suggesting that these antigen-presenting cells (APC) are targets of IFN-γ (Fig. 8a, b and Supplementary Fig. 19). Consistently, we observed a reduction of DC infiltration within the TME but an increased infiltration and maturation in tumor-derived lymph nodes (tdLN) post-M1-mutIL-18 treatment (Fig. 8c, d), indicating DC activation and migration from the TME to tdLNs. Concurrently with these, CD8+ T cells in tdLNs showed significant upregulation of activation markers CD69 and CD44 (Fig. 8e, f), demonstrating enhanced priming and activation of CD8+ T cells in the tdLNs. Previous data showed that activated CD8+ T cells highly expressed IL-18 receptors, here we also found that CD8+ T cells in the tdLN exhibited elevated expression of IL-18Rα (Fig. 8g). Similar patterns were observed in DCs and CD8+ T cells isolated from spleens following treatment with M1-mutIL-18 (Supplementary Fig. 20a–c). In vitro coculture experiments further confirmed that DCs promote CD8+ T cell activation and induce IL-18 receptor expression on CD8+ T cells (Fig. 8h, i and Supplementary Fig. 21a, b). Based on these findings, we hypothesize that activated CD8+ T cells in tdLNs and spleens, characterized by enhanced IL-18Rα expression, may migrate to the TME and serve as targets for mutIL-18 expressed by M1-mutIL-18, thereby establishing a positive feedback loop within the IL-18 pathway. Indeed, we observed elevated expression of CCL3-5, CCL9, CXCL9, CXCL16, and CX3CL1—chemokines responsible for CD8+ T cell recruitment[42,43]—in the TME, alongside increased IL-18Rα expression on CD8+ T cells following M1-mutIL-18 treatment (Fig. 8j–l and Supplementary Fig. 21c, d). In contrast, NK cells exhibited decreased IL-18Rα expression post-M1-mutIL-18 treatment without positive feedback (Supplementary Figs. 20d and 21e, f). Enhanced expression of IL-18 receptors on CD8+ T cells from tdLNs and spleen may ensure robust and sustained IFN-γ expression by mutIL-18 stimulation in TME.

In addition, intratumoral administration of M1-mutIL-18 induced significant CD8+ T cell infiltration in both injected and distant uninjected tumors, accompanied by a marked increase in the proportions of IL-18Rα+ CD8+ T cell and IFN-γ+ CD8+ T cells (Supplementary Fig. 22a–c). The expression of IFN-γ in these distant tumors were lower compared to those in OV-injected tumors, likely due to the localized expression of mutIL-18 at the injection site (Supplementary Fig. 22c, d). Consistently, intratumoral administration of M1-mutIL-18 effectively inhibited tumor growth in both injected and uninjected tumors, with more pronounced antitumor effects observed at the injection site (Supplementary Fig. 22e–g). These results suggest that M1-mutIL-18-induced DC activation in tdLNs and spleen primes tumor-specific CD8+ T cells, thereby contributing to the abscopal anti-tumor activity. Furthermore, the anti-tumor efficacy of M1-mutIL-18 was significantly reduced in batf3-/- mice (Fig. 8m, n), indicating that cDC1s are essential for M1-mutIL-18-mediated anti-tumor positive feedback loop.

## Amplifying the antitumor effects of M1-mutIL-18 via PD-L1 blockade

IFN-γ stimulation induces the expression of the immune checkpoint PD-L1 on various cells, thereby modulating immune activation[44]. In our study, we observed a significant increase in PD-L1 expression and PD-L1+ cell proportion following infection with M1-mutIL-18 (Fig. 9a, b and Supplementary Fig. 19). Consequently, the combination of PD-L1 antibody with M1-mutIL-18 significantly enhanced the antitumor

efficacy, achieving complete remission in 80% of mice in the PD-L1 inhibitor-resistant tumor model B16F10 (Fig. 9c, d). Given the development of exhausted phenotype of CD8+ T cells upon M1-mutIL-18 treatment, we hypothesized that PD-L1 blockade could reverse this exhaustion. Further flow cytometry analysis confirmed that M1-mutIL-18 treatment significantly upregulated the expression of PD-1 and TIM-3 on CD8+ T cells, and the proportions of PD-1+ CD8+ T cells, PD-1+ TIM-3+ CD8+ T cells and PD-1+ TIM-3+ LAG-3+ CD8+ T cells were also markedly increased. However, subsequent PD-L1 blockade reduced TIM-3 and LAG-3 expression and significantly decreased the proportion of these exhausted subsets (Fig. 9e–j and Supplementary Fig. 23a, b). In addition, PD-L1 blockade also reversed the exhaustion phenotype of CD4+ T cells (Supplementary Fig. 23c–h). These findings demonstrate that M1-mutIL-18-induced T cell exhaustion is not irreversible but rather represents a partially exhausted state that can be rescued by immune checkpoint inhibition.

## Discussion

Our study discovers that OVs (e.g., M1 and HSV-1) can enhance the expression of IL-18 receptors within the TME, making them a promising target for OVs-based therapies. By combining IL-18 ligand with OVs or engineering the cytokine directly into the genome of M1 virus, enhanced antitumor effects are achieved. Particularly noteworthy is the armed OV M1-mutIL-18, which demonstrates potent efficacy across multiple solid tumor types. The therapy prompts NK cells and CD8+ T cells to release persistent IFN-γ, mediating a robust antitumor effect. Moreover, CD8+ T cells exhibit enhanced activation and differentiation, contributing to increased cytotoxicity and the establishment of long-term tumor surveillance. Priming and activation of CD8+ T cells by DC in tdLN and spleen induce the expression of IL-18 receptors, potentially enhancing CD8+ T cell responsiveness to IL-18 ligand within the tumor. Our findings suggest a robust antitumor strategy by concurrently reprogramming essential components of the IL-18 pathway.

IL-18 is an important cytokine in the regulation of anti-tumor immunity, however, the clinical response to IL-18 cytokine therapy has been limited, initially thought to be due to the neutralizing effect of IL-18BP, which impedes effective IL-18 receptor binding[45–47]. Therefore, IL-18BP decoy-resistant IL-18 variants have been developed and are currently undergoing clinical validation[28]. In our research, we observed that the antitumor effects of decoy-resistant IL-18 variants (mutIL-18) alone, whether in "cold" B16F10 or "hot" tumors CT26, are not as effective as M1-mut-IL18. This suggests that simply supplementing cytokines may not fully exploit the antitumor potential of the IL-18 pathway. The superior response of CT26 to mutIL-18 compared to B16F10 indicates a correlation between IL-18 receptor expression and treatment responsiveness. Analysis of TCGA data revealed generally low IL-18 receptor expression in most solid tumors, suggesting that the efficacy of IL-18 ligand may be limited in tumors with low receptor expression levels. OVs effectively promote the expression of IL-18 receptors by stimulating DCs and induce CD8+ T cell priming and activation in tdLN and spleen, ultimately providing receptor-positive CD8+ T cells into the TME as target cells for IL-18 ligand. Previous studies have demonstrated that OVs possess immunogenic properties capable of promoting lymphocyte infiltration into the TME, thereby converting "cold" tumors into "hot" tumors and potentially enhancing the efficacy of immune checkpoint inhibitors[48]. Our findings suggest that OVs also facilitate the presence of IL-18 receptor-positive lymphocytes, highlighting OVs as promising partners for IL-18-based therapy.

Harnessing IL-18 as a stimulator to enhance the antitumor effect of CAR-T therapy has been reported[49,50]. However, when considering loading IL-18 ligand into OVs, it is crucial to use mutIL-18 rather than wtIL-18 to achieve the enhanced antitumor effect. We hypothesize that IL-18 released by CAR-T cells act in an autocrine manner by binding to IL-18 receptors on CAR-T cells. In contrast, IL-18 released by OVs
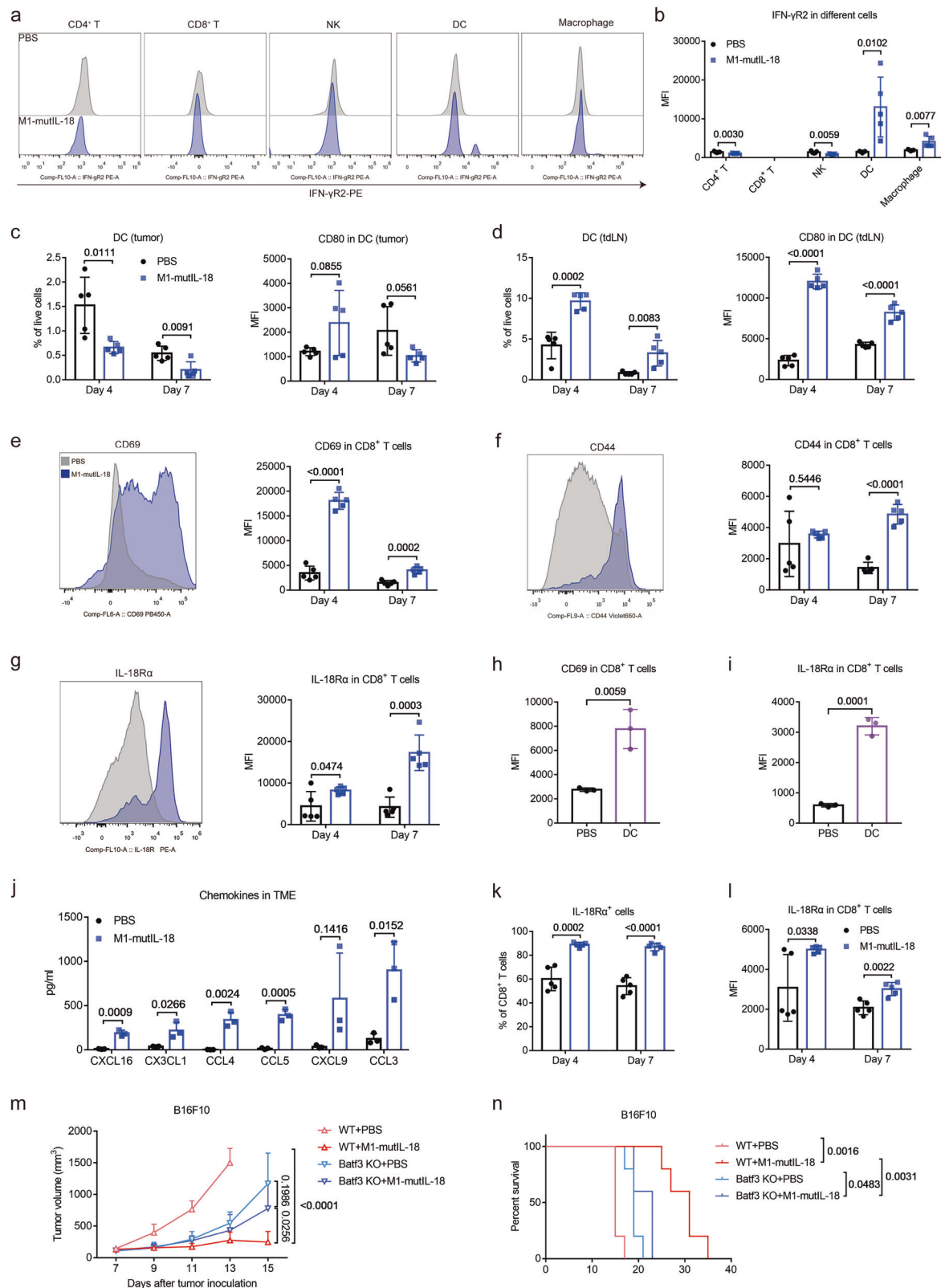
remains in the TME where it awaits recruitment of CD8^{+} T cells and NK cells to exert its function. The time gap between IL-18 expression and its binding to receptors provides an opportunity for IL-18BP to neutralize IL-18. IL-18BP is significantly induced by IL-18, potentially limiting its therapeutic efficacy. Therefore, in the context of OV therapy, mutIL-18, which is resistant to IL-18BP, serves as a more effective partner compared to wtIL-18. These results suggested that negative feedback mechanisms in the body could greatly limit the potentiation of cytokines on oncolytic viruses.

A notable observation was that CD8^{+} T cells undergo significant clonal expansion and differentiation within the M1-mutIL-18 group, distinct from the effector state observed in CD8^{+} T cells treated solely with the M1 virus. The substantial clonal expansion of CD8^{+} T cells, whether triggered by recognition of viral or tumor antigens, showed

**Fig. 8 | M1-mutIL-18 enhances IL-18 receptor on CD8$^+$ T cells via DC and creates a positive feedback loop. a–g, k-l** Female C57BL/6 J mice aged 4–6 weeks were implanted with B16F10 cells and treated with PBS or M1-mutIL-18 (1.5 × 10$^7$ PFU) via tail vein injection for 5 consecutive days. Mice were euthanized on day 4 and day 7 after the first dose administration. The number and function of immune cells in TME (**a–c**, **k-l**) and tdLN (**d–g**) were analyzed by flow cytometry. **a, b**, Representative flow plots (**a**) and MFI (**b**) of IFN-γR2 in different immune cells in TME. **c** Proportion and CD80 expression of DC cells in TME. **d** Proportion and CD80 expression of DC cells in tdLN. **e, f** MFI of CD69 (**e**) and CD44 (**f**) in CD8$^+$ T cells in tdLN. **g** MFI of IL-18Rα in CD8$^+$ T cells in tdLN. **h, i** MFI of CD69 (**h**) and IL-18Rα (**i**) in CD8$^+$ T cells that were co-cultured with DC for 48 h. CD8$^+$ T cells were isolated from untreated mice. **j** Expression of chemokines in TME. **k** Proportion of IL-18Rα$^+$ cells in CD8$^+$ T cells in TME. **l** MFI of IL-18Rα in CD8$^+$ T cells in TME. **m, n** Male C57BL/6j wild-type or batf3$^{-/-}$ mice aged 4–6 weeks were implanted with B16F10 cells and treated with PBS or M1-mutIL-18 (1.5 × 10$^7$ PFU) via tail vein injection for 5 consecutive days. Tumor growth was observed every 2 days. **c–g**, **k** the figure legends are same as in Fig. 8c. **a–l** The number of mice is the same as the individual data points in bar charts. **m, n** $n = 5$ mice per group. In all figures, data with error bars represent mean ± SD. $P$-values were calculated using unpaired, two-tailed Student's $t$-test (**b–m**) or log rank test (**n**).

high expression of effector molecules, indicative of a cytotoxic anti-tumor state. The full clonal expansion of CD8$^+$ T cells require the simultaneous presence of multiple signals, including TCR-mediated antigen recognition, co-stimulatory signals, and cytokine signals[51,52]. We hypothesize that enhanced priming and activation of CD8$^+$ T cells by DC in tdLN and spleen provides antigen-specific CD8$^+$ T cells in the TME, and the high concentration of mutIL-18 produced by M1-mutIL-18 within tumors combined with the inflammatory effect of M1 virus directly or indirectly drives potent CD8$^+$ T cell clonal expansion. Directly, while mutIL-18 released by the armed virus may directly interact with the enhanced IL-18 receptors on the surface of these CD8$^+$ T cells, providing cytokine signals. IL-18 has also been reported to promote CD8$^+$ T cell proliferation by stimulating the expansion of CD4$^+$ T cells[49]. However, the deletion of CD4$^+$ T cells did not affect the anti-tumor effect of M1-mutIL-18, suggesting that CD8$^+$ T cell expansion after M1-mutIL-18 treatment does not rely on CD4$^+$ T cells. Indirectly, IL-18 or M1 virus may enhance CD8$^+$ T cell clonal expansion by stimulating the release of IL-2, IL-12 or type I IFN, which requires further validation in the scenario of M1-mutIL-18[51,52]. As three TCR clones emerged as dominant, the clonal TCR diversity was reduced in the M1-mutIL-18 group compared to the M1 group. We propose that this reduction is driven by M1-mutIL-18 rather than the tumors themselves. In line with previous literature[53–55], clonal expansion of CD8$^+$ T cells against antigens initially generates diverse clonotypes, after which high-affinity clones are selectively expanded to become dominant. Thus, we suggest that the dominant clones observed in the M1-mutIL-18 group may emerge from peptide-MHC class I affinity screening, during which low-affinity clones are eliminated. While M1 virus treatment alone induces diverse clonotypes, likely representing the initial phase of CD8$^+$ T cell expansion, the addition of mutIL-18 may further accelerate the process of clonotype screening by promoting clonal expansion.

ScRNA-seq analysis revealed the emergence of a dual phenotype CD8$^+$ T cell subset following M1-mutIL-18 treatment, characterized by co-expression of both exhaustion and cytotoxic effector signatures. We propose that this dual-phenotype CD8$^+$ T cell subset is driven primarily by extensive CD8$^+$ T cell clonal expansion. As demonstrated by our data, exhausted CD8$^+$ T cells are predominantly composed of TCR clones 3, 55, and 163, which represent the most clonally expanded CD8$^+$ T cell populations within TME. Sustained clonal expansion may lead to the upregulation of exhaustion markers as a negative feedback mechanism to prevent excessive activation-induced immune damage[56,57]. However, these findings differ from those reported by Zhou et al., 2020, where decoy-resistant IL-18 (DR-18) was associated with clonal expansion of effector-type CD8$^+$ T cells, accompanied by a reduction in exhausted CD8$^+$ T cells[28]. We consider that this discrepancy may be attributable to the differences of clonal expansion extent. In Zhou et al., DR-18 protein was directly administered, whereas in our study, mutIL-18 was endogenously produced by an oncolytic virus replicating within tumors, likely leading to higher local protein concentrations. Additionally, the oncolytic virus itself is capable of promoting IL-18 receptor expression, which may further activate IL-18 pathway more potently to amplify CD8$^+$ T cell clonal expansion.

Therefore, the formation of dual-phenotype CD8$^+$ T cells following M1-mutIL-18 treatment reflects extensive CD8$^+$ T cell clonal expansion and a robust anti-tumor immune response within the TME. More importantly, similar to the results of PD-1 antibody in combination with IL-18 ligand[28], PD-L1 blockade effectively inhibits the formation of exhausted CD8$^+$ T cells and enhances the antitumor efficacy of M1-mutIL-18, demonstrating that M1-mutIL-18-induced CD8$^+$ T cell exhaustion is not irreversible but rather represents a partially exhausted state that can be rescued by immune checkpoint inhibition.

OVs as a promising tumor therapy, take the advantages of targeted therapy, gene therapy, and immunotherapy. By leveraging virus replicating within tumor tissues, loaded cytokines can be highly and specifically expressed at the tumor site, which not only reduces the toxicity of cytokine therapy but also alleviates patient burden. As we know, IL-18 serves as a crucial trigger for various autoimmune diseases[45,58]. In the setting of mutIL-18, the absence of negative feedback regulation by IL-18BP may lead to unintended immune activation beyond tumor-targeted organs, resulting in severe toxicity[59]. OV-mutIL-18 viruses are expected to achieve excellent anti-tumor effects while significantly mitigating the possible potential toxic effects associated with mutIL-18. Loading mutIL-18 into OV represents a safe and efficient method where mutIL-18 can be highly expressed during viral replication. Meanwhile, the combination of OVs and IL-18 ligands is a two-drug combination, which has lower off-target risk than other multi-drug combinations and is more suitable for application in clinical therapy.

In summary, we develop a potent immunotherapy by reprogramming key components of the IL-18 pathway, providing a new strategy for oncolytic virus engineering. T-VEC, which was approved by the FDA in 2015, is currently being evaluated in clinical trials with various combination therapy regimens. Additionally, IL-18BP decoy-resistant IL-18 variants are also undergoing clinical investigation (NCT06492707). Given the robust anti-tumor effects observed with HSV-1 combined with mutIL-18, there is strong rationale for the combination of T-VEC and IL-18BP decoy-resistant IL-18 variants. Our findings also demonstrate that intravenous injection of M1-mutIL-18 achieves robust antitumor effect comparable to intra-tumoral injection without causing obvious toxic effect, positioning it as an excellent candidate to overcome the primary limitation of oncolytic virus administration via intra-tumoral routes. Finally, our study suggests that unpaired changes in receptors and ligands can be previously overlooked but critical targets for tumor therapy.

## Methods
### Cell lines
B16F10 (CRL-6475), CT26 (CRL-2638), MC38 (CRL-2640), EMT6 (CRL-2755), BHK-21 (CCL-10), vero (CCL-81) were initially obtained from the American Type Culture Collection. GL261 cell line was kindly provided by Guangzhou Virotech Pharmaceutical Co., Ltd. The B16F10, CT26, MC38 and EMT6 cell lines was cultured in RPMI-1640 (Gibco, Carlsbad, CA) supplemented with 10% fetal bovine serum (Gibco) and 1×penicillin and 1% penicillin/streptomycin (Life Technologies, Carlsbad, CA). The other cell lines were cultured in DMEM (Gibco, Carlsbad, CA). All
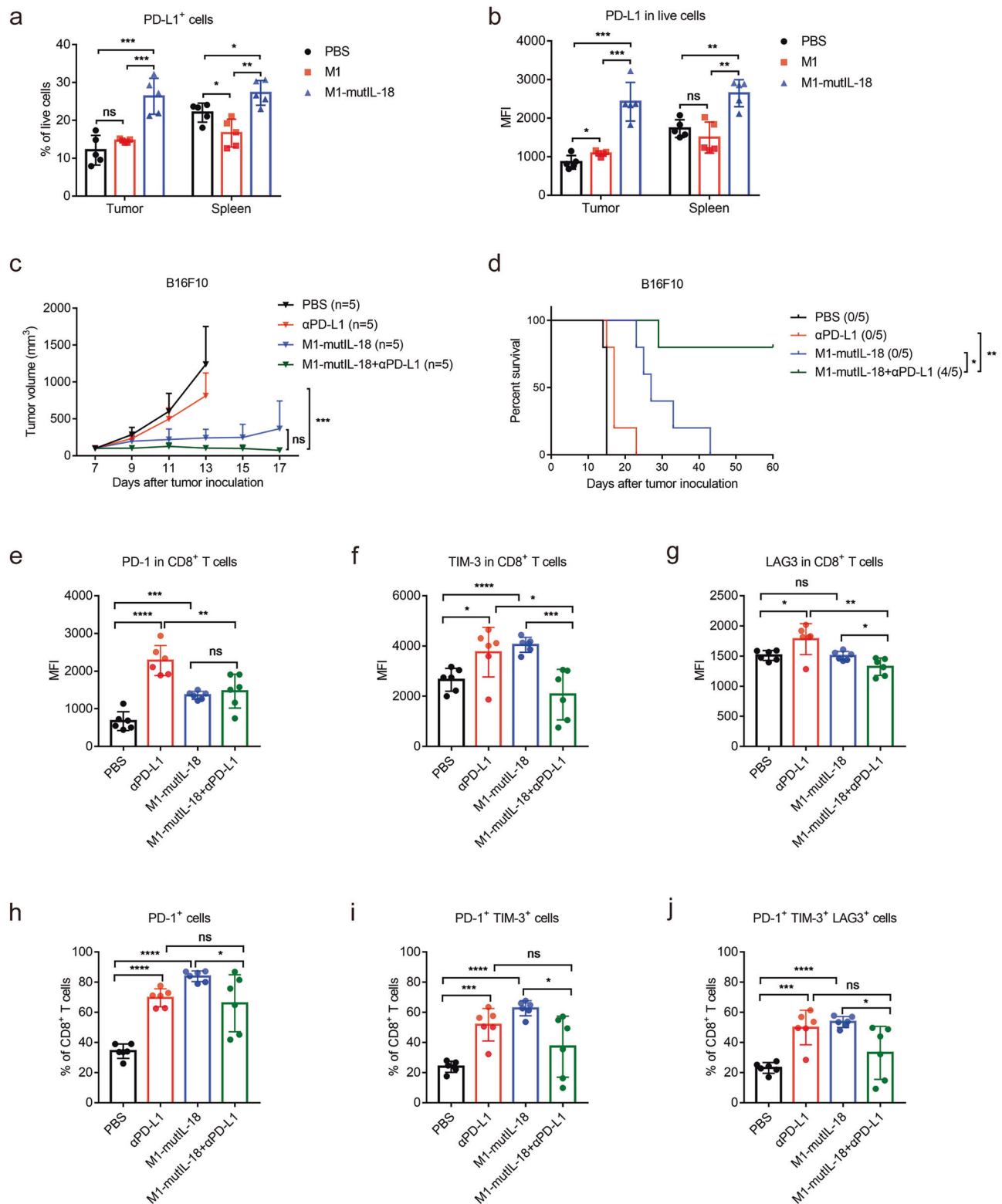
cells were cultured at 37 °C in a 5% $CO_2$ humidified atmosphere and kept at low passage once obtained from collaborators.

## Virus

Armed viruses used in this study were based on the M1 strain, which was described previously[29]. All transgenes were inserted between C and E3 of the M1 virus. The viruses were identified by PCR and western blot, respectively, to determine whether they were successfully constructed. The HSV-1 strain was supplied by Guangzhou Virotech

Pharmaceutical Co., Ltd. These viruses were produced by infecting Vero cells, and viral titers were determined by a CCID50 assay using BHK-21 cells.

## In vitro infection experiments

To examine the expression and biological activity of wtIL-18 and mutIL-18, using 0.001 MOI virus to infect B16F10 cells for 48 h, intracellular and extracellular protein expression was detected by Western blot and ELISA, respectively. Approximately $1 \times 10^6$ mouse spleen lymphocytes

**Fig. 9 | Amplifying the antitumor effects of M1-mutIL-18 via PD-L1 blockade.**
**a, b** Female C57BL/6 J mice aged 4−6 weeks were implanted with B16F10 cells and treated with PBS, M1 ($1.5 \times 10^7$ PFU) or M1-mutIL-18 ($1.5 \times 10^7$ PFU) via tail vein injection for 5 consecutive days. Mice were euthanized on day 4 and day 7 after the first dose administration. The expression of PD-L1 in tumor (day 4) and spleen (day 7) was analyzed by flow cytometry. Proportion of PD-L1$^+$ cells in live cells (**a**) and MFI of PD-L1 in live cells (**b**) are shown. **c, d** Female C57BL/6 J mice aged 4−6 weeks were implanted with B16F10 and treated with PBS or M1-mutIL-18 ($4 \times 10^6$ PFU) via tail vein injection for 5 consecutive days. On the day of the first administration of M1-mutIL-18, anti-PD-L1 antibody was intraperitoneally injected every 3 days for a total of 5 times. **e−j** Female C57BL/6 J mice aged 4−6 weeks were implanted with B16F10 and treated with PBS or M1-mutIL-18 ($1.5 \times 10^7$ PFU) via tail vein injection for 5 consecutive days. On the day of the first administration of M1-mutIL-18, anti-PD-L1 antibody was intraperitoneally injected every 3 days for a total of 3 times. Mice were euthanized on day 7 after the first dose administration. The number and function of immune cells in TME were analyzed by flow cytometry. **e−g** MFI of PD-1 (**e**), TIM-3 (**f**) or LAG3 (**g**) in CD8$^+$ T cells. **h−j** Proportion of PD-1$^+$ cells (**h**), PD-1$^+$ TIM-3$^+$ cells (**i**) or PD-1$^+$ TIM-3$^+$ LAG3$^+$cells (**j**) in CD8$^+$ T cells. **a, b, e−j** the number of mice is the same as the individual data points in bar charts. **c, d**, $n = 5$ mice per group. In all figures, data with error bars represent mean ± SD. ns, not significant. *$P < 0.05$, **$P < 0.01$, ***$P < 0.001$, ****$P < 0.0001$. $P$-values were calculated using unpaired, two-tailed Student's $t$-test (**a−c**, **e−j**) or log rank test (**d**).

were stimulated ex vivo with 4 ng/mL wtIL-18 and mutIL-18 expressed by M1-wtIL-18 or M1-mutIL-18. All stimulations were performed in the presence of mIL-12 (10 ng/ml, CT022-M08H, Sino Biological) for 4−6 h in RPMI containing 10% fetal bovine serum. IFN-γ production after stimulation was measured by ELISA.

To examine the replication kinetics of M1-wtIL-18 or M1-mutIL-18, using 0.01 MOI virus to infect B16F10 cells. Culture supernatants were collected at 6, 12, 24, 36, and 48 h, and virus titers were determined by tissue culture infectious dose 50 ($CCID_{50}$) assay in BHK-21 cells.

To examine the cell cytotoxicity of M1-wtIL-18 or M1-mutIL-18, using indicated MOI virus to infect B16F10 cells for 24 h. After infection, cell counting kit-8 (CCK8) (HY-K0301, MCE) was added to each well, and the cell viability was determined using a microplate reader (Synergy H1, BioTek), according to the manufacturer's instructions.

### Confocal microscopy imaging
To examine the expression mutIL-18, using 0.001 MOI M1-mutIL-18 to infect B16F10 cells for 48 h, PBS and M1 as a control. The infected cells were washed three times with pre-cooled PBS, fixed with 4% PFA for 20 min at room temperature, permeabilized with 0.1% Triton X-100 for 10 min, and blocked with 5% skimmed milk powder in PBS at 37 °C for 1 h. Then, the cells were incubated for 1 h at room temperature with mouse anti-P2A (MABS2005, Millipore) and rabbit anti-IL-18 (ab71495, abcam) antibody. After being washed three times with PBS, the cells were incubated for 15 min with FITC conjugated goat anti-mouse IgG (31547, Thermo Fisher) and Cyanine5 conjugated goat anti-rabbit IgG (A10523, Thermo Fisher). After being washed three times with PBS, the cells were incubated for 15 min with Hoechst 33342 (62249, Thermo Fisher). After being washed three times with PBS, the fluorescence images were recorded using a Nikon A1 confocal microscope (Nikon, Japan).

### Western blot
Cells were lysed by M-PER Mammalian Protein Extraction Reagent (Thermo Scientific). The protein lysate was resolved by SDS/PAGE, and analyzed by immunoblotting using primary antibodies specific for E1 protein of M1 (produced by Beijing Protein Innovation)[17–19], GAPDH (MA5-35235, Thermo Fisher), and P2A (MABS2005, Millipore), followed by appropriate HRP-conjugated secondary antibodies. Membranes were visualized on a ChemiDoc XRS+ System (Bio-Rad) using Immobilon Western Chemiluminescent HRP Substrate (Millipore).

### ELISA
IL-18, IL-18BP and IFN-γ ELISAs were performed using Mouse IL-18 ELISA Kit (P70380, RayBiotech or EK218, Multi sciences), Mouse IL-18 BPc ELISA Kit (Q9Z0M9, RayBiotech) and Mouse IFN-gamma ELISA Kit (EK280, Multi sciences) according to the manufacturers' instructions.

### Antibody array
Tumor samples were collected from tumor-bearing mice 7 d after M1-mutIL-18 treatment. For each sample, 50 μg total protein extracted from each sample was used to detect cytokines with mouse antibody array (QAM-CAA-4000, Raybiotech) according to the manufacturers' instructions.

### Animal experiments
Animal studies were approved by the Animal Ethical and Welfare Committee of Sun Yat-sen University. The maximal tumor burden is 3000 mm$^3$ permitted by ethics committee and we have adhered to these size limits in our experiments. Four- to six-week-old C57BL/6j mice (GDMLAC), BALB/c mice (GDMLAC), Rag1$^{-/-}$ mice (T004753, Gempharmatech Co., Ltd.) and Batf3$^{-/-}$ mice (NM-KO-190447, Shanghai Model Organisms Center, Inc.) were raised on a standard diet and water and a specific pathogen−free conditions and the experimental/control animals were bred separately. Moreover, mice were housed at an ambient temperature of 22-24 °C, humidity-controlled environment at 40%−70% under a 12 h light/dark cycle with ad libitum access to water and food. The number and sex of mice are shown in the figure legends. Gender analysis was not considered, as it had no significant effect on the efficacy of M1 and M1-mutIL-18. $1 \times 10^6$ B16F10 cells, $1 \times 10^6$ EMT6 cells, $1 \times 10^6$ CT26 cells, $2 \times 10^6$ GL261 cells and $2 \times 10^6$ MC38 cells were inoculated subcutaneously in the right flank. Unless otherwise noted, when tumors about 150 mm$^3$, the mice were randomized and the oncolytic virus were intravenously injected daily for a total of five doses. Virus titers were $4 \times 10^6$ PFU/mouse or $1.5 \times 10^7$ PFU/mouse as indicated in the related figure legends. WtIL-18 protein (0.32 mg/kg, produced by Sino Biological) and mutIL-18 (0.32 mg/kg, produced by Sino Biological) were intraperitoneally injected twice weekly for a total of 5 times. CD8a antibody (200 μg/mouse, clone 2.43, Bio X cell), CD4 antibody (200 μg/mouse, clone GK1.5, Bio X cell), NK1.1 antibody (200 μg/mouse, clone PK136, Bio X Cell), IFN-γ antibody (200 μg/mouse, clone R4-6A2, Bio X) and PD-L1 antibody (200 μg/mouse, clone B7-H1, Bio X Cell) were intraperitoneally injected every 3 day for a total of 5 times. Antibodies were administered 2 days before oncolytic virus therapy. WtIL-18 protein and mutIL-18 protein were administered on the day of oncolytic virus therapy. Control groups were treated with sterile PBS or isotype control antibodies. Tumor growth was measured using a digital caliper, and tumor volume was calculated by the formula: V = (length × width$^2$)/2. When plotting tumor growth curves, tumor sizes and body weights of each mouse were measured every 2 to 4 days, as shown in the corresponding figures; when plotting survival curves, tumor sizes and body weights of each mouse were measured every 1 or 2 days. Mice were euthanized by carbon dioxide inhalation when tumors reached the ethical endpoint (2000 mm$^3$), and the survival analyses reflect this endpoint unless the mice died before tumors reached the ethical endpoint. When tumor was not detected by palpation, mice were defined as cured.

To evaluate the efficacy of mutIL-18 in combination with M1 or HSV-1, mutIL-18 (0.32 mg/kg, produced by Sino Biological) was intraperitoneally injected twice weekly for a total of 5 times, M1 or HSV-1 ($2 \times 10^6$ pfu/mouse) was intratumorally injected only once. The remaining scenarios were consistent with the previous description.

For tumor re-challenge studies, mice exhibiting complete tumor regression were re-inoculated subcutaneously with twice the initial

dose about 34 days, 100 days, or 400 days after the initial tumors were cleared. As a control, age-matched treatment-naive mice were re-challenged at the same time. The remaining scenarios were consistent with the previous description.

## Analysis of Immunophenotype

Tumors, draining lymph nodes and spleens single-cell suspensions were prepared as described previously[23,30]. All samples were stained with Fixable Viability Stain 780 (565388, BD) and Fixable Viability Stain 700 (564997, BD) to identify dead cells and incubated with Fc receptor blocking antibody (553142, BD). Intracellular staining was performed by fixing and permeabilizing with the Transcription Factor Buffer Set (562574, BD). For endogenous cytokine production measurement, single-cell suspensions of tumor cells and splenocytes were incubated with Golgi-plug (555029, BD) for 4 h at 37 °C.

Cell staining was performed using the following fluorophore-conjugated antibodies purchased from BD or BioLegend: CD45 (30-f11, 563891, BD), CD3e (17A2, 561798, BD; 17A2, 560527, BD), CD8α (53-6.7, 561097, BD; 53-6.7, 564983, BD; 53-6.7, 557654, BD), CD4 (RM4-5, 100536, BioLegend; RM4-5, 100510, BioLegend; RM4-5, 100538, BioLegend), NK1.1 (PK136, 562921, BD; PK136, 562062, BD), IL-18Rα (A17071D, 157906, BioLegend; A17071D, 157904, BioLegend), IFN-γR2 (MOB-47, 113604, BioLegend), IFN-γ (XMG1.2, 505808, BioLegend), GZMB (QA16A02, 372212, BioLegend), TNF (MP6-XT22, 506308, BioLegend), CD69 (H1.2F3, 569688, BD; H1.2F3, 561932, BD; H1.2F3, 562920, BD), CD44 (IM7, 560570, BD; IM7, 740455, BD), CD62L (MEL-14, 563252, BD; MEL-14, 553151, BD), CD25 (3C7, 564370, BD), FOXP3 (MF23, 560408, BD), PD-L1 (10 F.9G2, 124334, BioLegend), CD11b (M1/70, 557960, BD; M1/70, 557657, BD), CD11c (N418, 561022, BD; HL3, 566504, BD), I-A/I-E (M5/114.15.2, 562363, BD; 2G9, 562009, BD), CD80 (16-10A1, 563687, BD; 16-10A1, 562611, BD), CD39 (Y23-1185, 567104, BD), PD-1 (29 F.1A12, 568868, BD), TIM-3 (RMT3-23, 119705, BioLegend), LAG3 (C9B7W, 125227, BioLegend). Fluorescence spectra were acquired and analysis by flow cytometry (CytoFLEX, Beckman Coulter). For flow cytometry analysis, Undyed or fluorescence minus one (FMO) staining was used for gating.

## Lymphocytotoxicity test

TDLN's lymphocytes and splenic lymphocytes were isolated with mouse lymphocytes separation kit (Dakewe, 7211011). Total lymphocytes were further enriched for T lymphocytes by EasySep™ Mouse T Cell Isolation Kit (19851, STEMCELL Technologies). Then, T lymphocytes were co-cultured with pre-seeded B16F10 cells for 3 days. Cells were washed with PBS for three times to remove the lymphocytes, the viability of tumor cells was detected by CCK8. Lymphocytotoxicity was calculated by the formula: Lymphocyto-toxicity = $(1\text{-}A_{tumor\ cells+lymphocytes}/A_{tumor\ cells}) \times 100\%$.

## DC-induced expression of IL-18Rα on T cells

Bone marrow cells were collected from the tibias and femurs of C57BL/6 J mice and cultured with RPMI-1640 medium containing 10% FBS, mGM-CSF (20 ng/ml, 315-03-250, PeproTech) and mIL-4 (10 ng/ml, 214-14-100, PeproTech). Fresh medium supplemented with mGM-CSF and mIL-4 was added on day 3, and half of the culture medium was replaced with fresh medium on day 5. DCs were harvested on day 7. Then, DCs were co-cultured with pre-seeded T cells for 2 days. T-cell function and expression of IL-18Rα were detected by flow cytometry.

## ScRNA-seq and scTCR-seq

Biological replicates from $n = 3$ pooled mice were processed for each experimental condition from B16F10 tumors. Tumor infiltrating CD45+ cells were sorted and purified. Biological replicates were then pooled together at the single-cell suspension stage with an equivalent number of cells from each replicate. The separated CD45+ cells were loaded into the Chromium instrument (10X Genomics, Pleasanton, CA), and

the resulting barcoded cDNAs were used to construct 5′ gene expression libraries and TCR enriched libraries. The libraries from each sample were then processed for RNA sequencing. Quality control and normalization were performed by NovelBio Co.,Ltd. with NovelBrain Cloud Analysis Platform (https://www.novelbrain.com/home/index). Seurat package (version: 4.1.1, https://satijalab.org/seurat/) was used for cell normalization and regression based on the expression table according to the UMI counts of each sample and percent of mitochondria rate to obtain the scaled data. Cell types were identified by using a combination of top expressed genes and canonical cell type marker genes. ScTCR-seq data was processed using CellRanger vdj v7.1.0 against the mouse VDJ reference provided by 10x Genomics. To identify differentially expressed genes among samples, the function FindMarkers with wilcox rank sum test algorithm was used under following criteria:1. $\log_2 FC > 0.25$; 2. $P$-value < 0.05; 3. min.pct > 0.1.

## Analysis of GEO data and TCGA data

The expression of cytokine receptors and ligands after treatment with M1 were obtained from GEO repository with accession code GSE152451. Human *Il18*, *Il18r1* and *Il18rap* expression in oHSV-1-treated recurrent glioblastoma patients were obtained from GEO repository with accession code GSE164104. Human *Il18r1* and *Il18rap* expression in multiple cancers and matched normal tissues were obtained from TCGA and GTEx projects and analysed by webserver GEPIA2. Overall Survival analysis based on gene expression of human *Il18*, *Il18r1* and *Il18rap* in skin cutaneous melanoma patients were analysed by web-server GEPIA2.

## Statistical analysis

Statistical analysis was conducted using GraphPad Prism 7 and 8 (GraphPad Software). Procedures of comparison and the numbers of animals in the experiment were described in each figure. Ordinary two-way ANOVA with Tukey's multiple comparisons test, two-tailed unpaired Student's $t$-test, log-rank testing or Pearson's correlation coefficient analysis (see Figure legends) were used to determine statistical significance (*$P < 0.05$, **$P < 0.01$, ***$P < 0.001$, ****$P < 0.0001$). No statistical methods were used to predetermine sample size.

## Data availability

The raw data of scRNA-seq and scTCR-seq have been deposited in GEO database under the accession codes GSE295936 (https://www.ncbi.nlm.nih.gov/geo). All data are included in the Supplementary Information or available from the authors, as are unique reagents used in this Article. The raw numbers for charts and graphs are available in the Source Data file whenever possible. Source data are provided with this paper.

## References

1. Galluzzi, L., Humeau, J., Buqué, A., Zitvogel, L. & Kroemer, G. Immunostimulation with chemotherapy in the era of immune checkpoint inhibitors. *Nat. Rev. Clin. Oncol.* **17**, 725–741 (2020).
2. Kwok, G., Yau, T. C., Chiu, J. W., Tse, E. & Kwong, Y. L. Pembrolizumab (Keytruda). *Hum. Vaccines Immunother.* **12**, 2777–2789 (2016).
3. Sznol, M. & Chen, L. Antagonist antibodies to PD-1 and B7-H1 (PD-L1) in the treatment of advanced human cancer. *Clin. Cancer Res.: Off. J. Am. Assoc. Cancer Res.* **19**, 1021–1034 (2013).
4. Kaufman, H. L., Kohlhapp, F. J. & Zloza, A. Oncolytic viruses: a new class of immunotherapy drugs. *Nat. Rev. Drug Discov.* **14**, 642–662 (2015).
5. Brown, M. C. et al. Cancer immunotherapy with recombinant poliovirus induces IFN-dominant activation of dendritic cells and tumor antigen-specific CTLs. *Sci. Transl. Med.* **9**, eaan4220 (2017).
6. Killock, D. Skin cancer: T-VEC oncolytic viral therapy shows promise in melanoma. *Nat. Rev. Clin. Oncol.* **12**, 438 (2015).

7. Hou, W., Sampath, P., Rojas, J. J. & Thorne, S. H. Oncolytic virus-mediated targeting of PGE2 in the tumor alters the immune status and sensitizes established and resistant tumors to immunotherapy. *Cancer cell* **30**, 108–119 (2016).

8. Zamarin, D. et al. Intratumoral modulation of the inducible co-stimulator ICOS by recombinant oncolytic virus promotes systemic anti-tumour immunity. *Nat. Commun.* **8**, 14340 (2017).

9. Kroemer, G. & Zitvogel, L. Leptin-producing oncolytic virus makes tumor-infiltrating T cells fit, not fat. *Immunity* **51**, 423–425 (2019).

10. Rivadeneira, D. B. et al. Oncolytic viruses engineered to enforce leptin expression reprogram tumor-infiltrating t cell metabolism and promote tumor clearance. *Immunity* **51**, 548–560.e544 (2019).

11. Soliman, H. et al. Oncolytic T-VEC virotherapy plus neoadjuvant chemotherapy in nonmetastatic triple-negative breast cancer: a phase 2 trial. *Nat. Med.* **29**, 450–457 (2023).

12. Chesney, J. A. et al. Randomized, double-blind, placebo-controlled, global phase III trial of talimogene laherparepvec combined with pembrolizumab for advanced melanoma. *J. Clin. Oncol.: Off. J. Am. Soc. Clin. Oncol.* **41**, 528–540 (2023).

13. Ribas, A. et al. Oncolytic virotherapy promotes intratumoral T cell infiltration and improves anti-PD-1 immunotherapy. *Cell* **170**, 1109–1119.e1110 (2017).

14. Dummer, R. et al. Neoadjuvant talimogene laherparepvec plus surgery versus surgery alone for resectable stage IIIB-IVM1a melanoma: a randomized, open-label, phase 2 trial. *Nat. Med.* **27**, 1789–1796 (2021).

15. Shalhout, S. Z., Miller, D. M., Emerick, K. S. & Kaufman, H. L. Therapy with oncolytic viruses: progress and challenges. *Nat. Rev. Clin. Oncol.* **20**, 160–177 (2023).

16. Li, Y. Y. et al. From discovery to spread: the evolution and phylogeny of Getah virus. *Infect., Genet. Evolution J. Mol. Epidemiol. Evolut. Genet. Infect. Dis.* **55**, 48–55 (2017).

17. Lin, Y. et al. Identification and characterization of alphavirus M1 as a selective oncolytic virus targeting ZAP-defective human cancers. *Proc. Natl. Acad. Sci. USA* **111**, E4504–E4512 (2014).

18. Zhang, H. et al. Targeting VCP enhances anticancer activity of oncolytic virus M1 in hepatocellular carcinoma. *Sci. Transl. Med.* **9**, eaam7996 (2017).

19. Guo, L. et al. Directed natural evolution generates a next-generation oncolytic virus with a high potency and safety profile. *Nat. Commun.* **14**, 3410 (2023).

20. Zhang, H. et al. Naturally existing oncolytic virus M1 is non-pathogenic for the nonhuman primates after multiple rounds of repeated intravenous injections. *Hum. gene Ther.* **27**, 700–711 (2016).

21. Cai, J. et al. Systematic characterization of the biodistribution of the oncolytic virus M1. *Hum. Gene Ther.* **31**, 1203–1213 (2020).

22. Song, D. et al. Identification of the receptor of oncolytic virus M1 as a therapeutic predictor for multiple solid tumors. *Signal Transduct. Target. Ther.* **7**, 100 (2022).

23. Dan, J. et al. Oncolytic virus M1 functions as a bifunctional checkpoint inhibitor to enhance the antitumor activity of DC vaccine. *Cell Rep. Med.* **4**, 101229 (2023).

24. Liu, Y. et al. Intravenous injection of the oncolytic virus M1 awakens antitumor T cells and overcomes resistance to checkpoint blockade. *Cell Death Dis.* **11**, 1062 (2020).

25. Tarhini, A. A. et al. A phase 2, randomized study of SB-485232, rhIL-18, in patients with previously untreated metastatic melanoma. *Cancer* **115**, 859–868 (2009).

26. Robertson, M. J. et al. Clinical and biological effects of recombinant human interleukin-18 administered by intravenous infusion to patients with advanced cancer. *Clin. Cancer Res. Off. J. Am. Assoc. Cancer Res.* **12**, 4265–4273 (2006).

27. Robertson, M. J. et al. A dose-escalation study of recombinant human interleukin-18 using two different schedules of administration in patients with cancer. *Clin. Cancer Res. Off. J. Am. Assoc. Cancer Res.* **14**, 3462–3469 (2008).

28. Zhou, T. et al. IL-18BP is a secreted immune checkpoint and barrier to IL-18 immunotherapy. *Nature* **583**, 609–614 (2020).

29. Zhu, W. et al. Real-time visualization and quantification of oncolytic M1 virus In vitro and in vivo. *Hum. gene Ther.* **32**, 158–165 (2021).

30. Liu, Y. et al. Overcoming resistance to oncolytic virus M1 by targeting PI3K-γ in tumor-associated myeloid cells. *Mol. Ther. J. Am. Soc. Gene Ther.* **30**, 3677–3693 (2022).

31. de Jong, L. C., Crnko, S., Ten Broeke, T. & Bovenschen, N. Non-cytotoxic functions of killer cell granzymes in viral infections. *PLoS Pathog.* **17**, e1009818 (2021).

32. Joeckel, L. T. et al. Mouse granzyme K has pro-inflammatory potential. *Cell Death Differ.* **18**, 1112–1119 (2011).

33. Jonsson, A. H. et al. Granzyme K(+) CD8 T cells form a core population in inflamed human tissue. *Sci. Transl. Med.* **14**, eabo0686 (2022).

34. Khan, O. et al. TOX transcriptionally and epigenetically programs CD8(+) T cell exhaustion. *Nature* **571**, 211–218 (2019).

35. Akbar, A. N. & Henson, S. M. Are senescence and exhaustion intertwined or unrelated processes that compromise immunity?. *Nat. Rev. Immunol.* **11**, 289–295 (2011).

36. Zhang, Z. et al. Efficacy of CTLA-4 checkpoint therapy is dependent on IL-21 signaling to mediate cytotoxic reprogramming of PD-1(+) CD8(+) T cells. *Nat. Immunol.* **26**, 92–104 (2025).

37. Sekine, T. et al. TOX is expressed by exhausted and polyfunctional human effector memory CD8(+) T cells. *Sci. Immunol.* **5**, eaba7918 (2020).

38. Minnie, S. A. et al. TIM-3(+) CD8 T cells with a terminally exhausted phenotype retain functional capacity in hematological malignancies. *Sci. Immunol.* **9**, eadg1094 (2024).

39. Figueiredo, C. M. et al. Mayaro virus replication restriction and induction of muscular inflammation in mice are dependent on age, type-I interferon response, and adaptive immunity. *Front. Microbiol.* **10**, 2246 (2019).

40. Hick, T. A. H. et al. Safety concern of recombination between self-amplifying mRNA vaccines and viruses is mitigated in vivo. *Mol. Ther. J. Am. Soc. Gene Ther.* **32**, 2519–2534 (2024).

41. Poo, Y. S. et al. Multiple immune factors are involved in controlling acute and chronic chikungunya virus infection. *PLoS Neglected Tropical Dis.* **8**, e3354 (2014).

42. Ozga, A. J., Chow, M. T. & Luster, A. D. Chemokines and the immune response to cancer. *Immunity* **54**, 859–874 (2021).

43. Castellino, F. et al. Chemokines enhance immunity by guiding naive CD8+ T cells to sites of CD4+ T cell-dendritic cell interaction. *Nature* **440**, 890–895 (2006).

44. Gocher, A. M., Workman, C. J. & Vignali, D. A. A. Interferon-γ: teammate or opponent in the tumour microenvironment?. *Nat. Rev. Immunol.* **22**, 158–172 (2022).

45. Landy, E., Carol, H., Ring, A. & Canna, S. Biological and clinical roles of IL-18 in inflammatory diseases. *Nat. Rev. Rheumatol.* **20**, 33–47 (2024).

46. Markowitz, G. J. et al. Inflammation-dependent IL18 signaling restricts hepatocellular carcinoma growth by enhancing the accumulation and activity of tumor-infiltrating lymphocytes. *Cancer Res.* **76**, 2394–2405 (2016).

47. Mutala, L. B. et al. The caspase-1/IL-18 axis of the inflammasome in tumor cells: a modulator of the Th1/Tc1 response of tumor-infiltrating t lymphocytes in colorectal cancer. *Cancers* **13**, 189 (2021).

48. Melcher, A., Harrington, K. & Vile, R. Oncolytic virotherapy as immunotherapy. *Science* **374**, 1325–1326 (2021).

49. Hu, B. et al. Augmentation of antitumor immunity by human and mouse CAR T cells secreting IL-18. *Cell Rep.* **20**, 3025–3033 (2017).

50. Chmielewski, M. & Abken, H. CAR T cells releasing IL-18 convert to T-Bet(high) FoxO1(low) effectors that exhibit augmented activity against advanced solid tumors. *Cell Rep.* **21**, 3205–3219 (2017).

51. Curtsinger, J. M. & Mescher, M. F. Inflammatory cytokines as a third signal for T cell activation. *Curr. Opin. Immunol.* **22**, 333–340 (2010).

52. Kalia, V. & Sarkar, S. Regulation of effector and memory CD8 T cell differentiation by IL-2-A balancing act. *Front. Immunol.* **9**, 2987 (2018).

53. Schober, K. et al. Reverse TCR repertoire evolution toward dominant low-affinity clones during chronic CMV infection. *Nat. Immunol.* **21**, 434–441 (2020).

54. Tscharke, D. C., Croft, N. P., Doherty, P. C. & La Gruta, N. L. Sizing up the key determinants of the CD8(+) T cell response. *Nat. Rev. Immunol.* **15**, 705–716 (2015).

55. Day, E. K. et al. Rapid CD8+ T cell repertoire focusing and selection of high-affinity clones into memory following primary infection with a persistent human virus: human cytomegalovirus. *J. Immunol.* **179**, 3203–3213 (2007).

56. McLane, L. M., Abdel-Hakeem, M. S. & Wherry, E. J. CD8 T cell exhaustion during chronic viral infection and cancer. *Annu. Rev. Immunol.* **37**, 457–495 (2019).

57. Yost, K. E. et al. Clonal replacement of tumor-specific T cells following PD-1 blockade. *Nat. Med.* **25**, 1251–1259 (2019).

58. Kaplanski, G. Interleukin-18: Biological properties and role in disease pathogenesis. *Immunol. Rev.* **281**, 138–153 (2018).

59. Dixon, K. O. & Kuchroo, V. K. IL-18: throwing off the shackles to boost anti-tumor immunity. *Cell Res.* **30**, 831–832 (2020).

## Author contributions

Conceptualization: Z.F., J.L., Y.Lin., Ying.L., and G.Y. Methodology: Z.F., C.H., X.T., Yang.L., L.H., and S.H. Investigation: Z.F., X.Lin., J.Z., J.Chen., X.Liu., X.C., and X.Liang. Formal analysis: Z.F., C.G., and C.X. Supervision: L.G., W.Z., J.H, J.L, and J.C. Writing–Original Draft: Z.F. Writing–Review & Editing: J.L, J.C and S.Y.

## Competing interests

Authors declare that they have no competing interests.

## Additional information

**Supplementary information** The online version contains supplementary material available at https://doi.org/10.1038/s41467-025-61439-0.

**Correspondence** and requests for materials should be addressed to Jing Cai or Jiankai Liang.

**Peer review information** *Nature Communications* thanks Howard Kaufman, Jonathan Pol and Raymond J. Winquist for their contribution to the peer review of this work. A peer review file is available.

**Reprints and permissions information** is available at http://www.nature.com/reprints

**Publisher's note** Springer Nature remains neutral with regard to jurisdictional claims in published maps and institutional affiliations.